

Unfitted finite element methods for axisymmetric two-phase flow

Harald Garcke · Robert Nürnberg · Quan Zhao

Received: date / Accepted: date

Abstract We propose and analyze unfitted finite element approximations for the two-phase incompressible Navier–Stokes flow in an axisymmetric setting. The discretized schemes are based on an Eulerian weak formulation for the Navier–Stokes equation in the 2d-meridian halfplane, together with a parametric formulation for the generating curve of the evolving interface. We use lowest order Taylor–Hood and piecewise linear elements for discretizing the Navier–Stokes formulation in the bulk and the moving interface, respectively. We discuss a variety of schemes, amongst which is a linear scheme that enjoys an equidistribution property on the discrete interface and good volume conservation. An alternative scheme can be shown to be unconditionally stable and to conserve the volume of the two phases exactly. Numerical results are presented to show the robustness and accuracy of the introduced methods for simulating both rising bubble and oscillating droplet experiments.

Keywords two-phase flow · axisymmetry · finite element method · stability · volume preservation · XFEM

Mathematics Subject Classification (2020) 76T06 · 76M10 · 35R35

1 Introduction

Two-phase flows are widely observed phenomena in nature, and they have important applications in industrial engineering and scientific experiments. Numerical approxi-

Harald Garcke
Fakultät für Mathematik, Universität Regensburg, 93040 Regensburg, Germany.
E-mail: harald.garcke@ur.de

Robert Nürnberg
Dipartimento di Matematica, Università di Trento, 38123 Trento, Italy.
E-mail: robert.nurnberg@unitn.it

Quan Zhao
Fakultät für Mathematik, Universität Regensburg, 93040 Regensburg, Germany.
E-mail: quan.zhao@ur.de

mations of these flows have attracted a lot of attention, and a large body of numerical methods have been introduced in recent decades, see e.g., [2, 3, 5, 10, 11, 18, 19, 21–23, 25, 26, 29, 31, 32, 35, 42–45, 48, 50, 51, 53–55, 57]. Nevertheless, accurate and efficient numerical approximations for fully three-dimensional flows remain a significant challenge. This is despite several different treatments of the moving interface being available in the literature. Among these one of the prominent methods is the so-called level set method [29, 42, 43, 50, 53], where the interface is represented as a level set function. The main drawback in this approach is that the level set function needs to be re-initialized constantly in order to stay close to the signed distance function. This usually introduces unphysical shifting of the interface, thus causing significant volume loss [27]. On the other hand, the front-tracking method, which tracks the interface explicitly with a set of markers or a lower-dimensional mesh, provides a very accurate approximation of the interface and in particular the volume preservation aspect, see [10, 11, 26]. However, the front tracking method may struggle with complicated mesh manipulations which are often necessary, for example, in the computation of interface-bulk cross terms in the unfitted mesh approach [9, 11] or during the dynamic control of the bulk and interface meshes in the moving fitted mesh approach [4, 46].

The computationally challenging aspect of fully three-dimensional two-phase flows not only comes from the large size of the problem itself but also involves the possible difficulties of the numerical methods themselves, see e.g., [27, 30, 41]. Fortunately, in many situations the two-phase flow satisfies a rotational symmetry, meaning that the complex 3d problem can be reduced to a much simpler two-dimensional problem in the meridian halfplane. Moreover, the evolving fluid interface can be modelled by a one-dimensional generating curve, dramatically reducing the computational complexity. For front tracking methods, in particular, dealing with a discrete curve avoids undesirable mesh distortions as well as the associated remedies like mesh quality controls. There exist several numerical approximations for the axisymmetric two-phase incompressible flows, including the level set method [17, 52], the diffuse-interface approach [34, 38] and the moving mesh interface-tracking method [24, 28]. The main aim of this work is to explore unfitted finite element approximations for the axisymmetric two-phase incompressible flow and pay particular attention to energy stability and volume preservation aspects. The numerical methods we consider fall into the framework of a parametric approach, which was introduced in [10, 11] by Barrett, Garcke and Nürnberg, see (2.6c)-(2.6d). In this ‘BGN’ approach, the surface tension force is accurately computed with the help of a curvature identity, see [20]. For the evolving interface, the normal velocity is prescribed by the normal part of the fluid velocity, which allows tangential degrees of freedoms to improve the quality of the interface mesh. In particular, for an evolving curve, a semidiscrete version of the discretized scheme leads to uniformly distributed mesh points [8]. The interested reader is referred to the recent review paper [14] for a detailed discussion of this tangential velocity. We also note that, in the context of geometric flows, alternative approaches that also introduce a benign tangential velocity have been considered in [33, 40].

The unfitted finite element approximations we introduce in this paper crucially rely on an appropriate formulation of the surface tension forces in the axisymmet-

ric setting. Here we rely on two possible formulations for the mean curvature of the interface presented in [12, 13]. The first formulation leads to a discretization of the curvature of the generating curve, thus providing an equidistribution property as in the two-dimensional case, see [8, 11]. The alternative is to approximate the mean curvature of the three-dimensional interface, which has the advantage that an unconditional stability estimate can be shown. The overall numerical methods are then obtained by coupling the interface evolution to the fluid flow in the bulk. We follow the approach from the unfitted 2d/3d approximations of the Eulerian weak formulation that was introduced in [11]. In particular, by employing a special XFEM enrichment procedure for the pressure space, a volume preservation property can be shown on the semidiscrete level.

Strengthening the volume conservation property to the fully discrete level is also possible, on combining the XFEM technique with discrete time-weighted interface normals as derived in [6]. These time-weighted interface approximations were initially explored in the context of the surface diffusion flow [7, 37] and then extended to the axisymmetric geometric flows in [6]. In the 2d/3d setting an exactly volume-preserving finite element method for the two-phase incompressible flow was recently proposed by the authors in [26].

The rest of the paper is organized as follows. In Section 2, we review an Eulerian weak formulation for the sharp-interface model of two-phase incompressible flow in three dimensions. Next, in Section 3, we introduce two axisymmetric weak formulations for the considered flow under a suitable axisymmetric setting. Subsequently, in Section 4, we propose four discretized schemes based on the axisymmetric formulations and analyze their properties of equidistribution, energy stability and volume preservation. Numerical results for rising bubble and oscillating droplet experiments are presented in Section 5 to show the robustness and the accuracy of the introduced schemes. Finally, we draw some conclusions in Section 6.

2 Mathematical formulations in 3d

We consider the dynamics of the two-phase fluids in a fixed bounded domain $\Omega \subset \mathbb{R}^3$ with $\Omega = \Omega_+(t) \cup \Omega_-(t) \cup S(t)$, where $\Omega_{\pm}(t) \subset \mathbb{R}^3$ are the regions occupied by the two fluids, t is the time variable, and $S(t)$ is a closed surface representing the fluid interface which separates the two regions. In the following we stay close to the presentation in [11], see also [30]. We assume a parameterization of $S(t)$ is given by: $\vec{\mathcal{Y}}(\cdot, t) : \mathcal{O} \rightarrow \mathbb{R}^3$, where \mathcal{O} is the reference surface. The induced interface velocity is then defined as

$$\vec{\mathcal{V}}(\vec{\mathcal{Y}}(\vec{q}, t), t) = \partial_t \vec{\mathcal{Y}}(\vec{q}, t) \quad \forall \vec{q} \in \mathcal{O}.$$

Moreover, we introduce the mean curvature of the interface as

$$\mathcal{H} \vec{n}_s = \Delta_s \vec{\text{id}}, \quad (2.1)$$

where \vec{n}_s is the unit normal to $S(t)$ and points to the region $\Omega_+(t)$, $\Delta_s = \nabla_s \cdot \nabla_s$ is the surface Laplacian operator on the surface with ∇_s being the surface gradient, and $\vec{\text{id}}$ is the identity function on $S(t)$.

Let $\check{u}(\cdot, t) : \Omega \times [0, T] \rightarrow \mathbb{R}^3$ be the fluid velocity, and $\check{p}(\cdot, t) : \Omega \times [0, T] \rightarrow \mathbb{R}$ be the pressure. Moreover, we use ρ_{\pm} and μ_{\pm} to denote the densities and viscosities of the fluids in $\Omega_{\pm}(t)$, respectively. Then the governing equations for the two-phase Navier–Stokes flow are given by

$$\rho_{\pm}(\partial_t \check{u} + \check{u} \cdot \nabla \check{u}) = \nabla \cdot \underline{\underline{\sigma}} + \rho_{\pm} \check{g} \quad \text{in } \Omega_{\pm}(t), \quad (2.2a)$$

$$\nabla \cdot \check{u} = 0 \quad \text{in } \Omega_{\pm}(t), \quad (2.2b)$$

$$[\check{u}]_{-}^{+} = 0 \quad \text{on } S(t), \quad (2.2c)$$

$$[\underline{\underline{\sigma}} \check{n}_s]_{-}^{+} = -\gamma \mathcal{H} \check{n}_s \quad \text{on } S(t), \quad (2.2d)$$

$$\check{\mathcal{V}} \cdot \check{n}_s = \check{u} \cdot \check{n}_s \quad \text{on } S(t), \quad (2.2e)$$

$$\check{u} = \vec{0} \quad \text{on } \partial_1 \Omega, \quad (2.2f)$$

$$\check{u} \cdot \check{n}_b = 0, \quad (\underline{\underline{\sigma}} \check{n}_b) \cdot \vec{t} = 0 \quad \forall \vec{t} \in \{\check{n}_b\}^{\perp} \quad \text{on } \partial_2 \Omega. \quad (2.2g)$$

Here (2.2a)–(2.2b) are the two-phase Navier–Stokes equations, \check{g} is the body acceleration, $\underline{\underline{\sigma}}$ is the stress tensor defined by

$$\underline{\underline{\sigma}} = \mu_{\pm} [\nabla \check{u} + (\nabla \check{u})^T] - \check{p} \underline{\underline{I}}_3 = 2\mu_{\pm} \underline{\underline{D}}(\check{u}) - \check{p} \underline{\underline{I}}_3 \quad \text{in } \Omega_{\pm}(t),$$

with $\underline{\underline{D}}(\check{u}) = \frac{1}{2} [\nabla \check{u} + (\nabla \check{u})^T]$ being the strain rate, and $\underline{\underline{I}}_3 \in \mathbb{R}^{3 \times 3}$ is the identity matrix. Equations (2.2c)–(2.2e) are the classical interface conditions, where $[\cdot]_{-}^{+}$ denotes the jump value from $\Omega_{-}(t)$ to $\Omega_{+}(t)$, γ is the surface tension of $S(t)$. Moreover, we prescribe the no slip condition (2.2f) on $\partial_1 \Omega$ and a free slip condition (2.2g) on $\partial_2 \Omega$, where \check{n}_b is the outer unit normal to $\partial \Omega$, and $\{\check{n}_b\}^{\perp} := \{\vec{t} \in \mathbb{R}^3 : \vec{t} \cdot \check{n}_b = 0\}$.

We define the total energy of the system as

$$\mathcal{E}(t) = \frac{1}{2} \int_{\Omega_{+}(t)} \rho_{+} |\check{u}|^2 dV + \frac{1}{2} \int_{\Omega_{-}(t)} \rho_{-} |\check{u}|^2 dV + \gamma |S(t)|, \quad (2.3)$$

where $|S(t)| = \int_{S(t)} 1 dS$. Then the dynamic system obeys the volume conservation and energy laws as follows

$$\frac{d}{dt} \text{vol}(\Omega_{-}(t)) = \int_{S(t)} \check{\mathcal{V}} \cdot \check{n}_s dS = \int_{\Omega_{-}(t)} \nabla \cdot \check{u} dV = 0, \quad (2.4a)$$

$$\frac{d}{dt} \mathcal{E}(t) = -2 \int_{\Omega} \mu \underline{\underline{D}}(\check{u}) : \underline{\underline{D}}(\check{u}) dV + \int_{\Omega} \rho \check{g} \cdot \check{u} dV, \quad (2.4b)$$

where we introduced $\rho(\cdot, t) = \rho_{+} \mathcal{X}_{\Omega_{+}(t)} + \rho_{-} \mathcal{X}_{\Omega_{-}(t)}$ and $\mu(\cdot, t) = \mu_{+} \mathcal{X}_{\Omega_{+}(t)} + \mu_{-} \mathcal{X}_{\Omega_{-}(t)}$ with \mathcal{X}_E being the characteristic function of a set E .

We denote by $(\cdot, \cdot)_{\Omega}$ and $\langle \cdot, \cdot \rangle_{S(t)}$ the L^2 -inner products over Ω and $S(t)$, respectively. On defining the function spaces

$$\check{\mathcal{U}} = \{\vec{\chi} \in [H^1(\Omega)]^3 : \vec{\chi} = 0 \text{ on } \partial_1 \Omega, \quad \vec{\chi} \cdot \check{n}_b = 0 \text{ on } \partial_2 \Omega\},$$

$$\check{\mathcal{P}} = \{\eta \in L^2(\Omega) : (\eta, 1)_{\Omega} = 0\}, \quad \check{\mathcal{V}} := H^1(0, T; [L^2(\Omega)]^3) \cap L^2(0, T; \check{\mathcal{U}}),$$

we then recall the following Eulerian weak formulation for the two-phase incompressible flow from [11, (3.9)]. Given the initial velocity $\check{\mathbf{u}}_0 = \check{\mathbf{u}}(\cdot, 0)$ and the fluid interface $S(0)$, we find $S(t) = \check{\mathcal{V}}(\mathcal{O}, t)$ with $\check{\mathcal{V}}(\cdot, t) \in [L^2(S(t))]^3$, $\check{\mathbf{u}} \in \check{\mathbb{V}}$, $\check{p} \in L^2(0, T; \check{\mathbb{P}})$, and $\mathcal{H}(\cdot, t) \in L^2(S(t))$ such that for all $t \in (0, T]$

$$\begin{aligned} & \frac{1}{2} \left[\frac{d}{dt} (\rho \check{\mathbf{u}}, \check{\chi})_{\Omega} + (\rho \partial_t \check{\mathbf{u}}, \check{\chi})_{\Omega} - (\rho \check{\mathbf{u}}, \partial_t \check{\chi})_{\Omega} \right] + 2(\mu \mathbb{D}(\check{\mathbf{u}}), \mathbb{D}(\check{\chi}))_{\Omega} \\ & + \frac{1}{2} \left[(\rho [\check{\mathbf{u}} \cdot \nabla] \check{\mathbf{u}}, \check{\chi})_{\Omega} - (\rho [\check{\mathbf{u}} \cdot \nabla] \check{\chi}, \check{\mathbf{u}})_{\Omega} \right] - (\check{p}, \nabla \cdot \check{\chi})_{\Omega} \\ & - \gamma \langle \mathcal{H} \check{\mathbf{n}}_s, \check{\chi} \rangle_{S(t)} = (\rho \check{\mathbf{g}}, \check{\chi})_{\Omega} \quad \forall \check{\chi} \in \check{\mathbb{V}}, \end{aligned} \quad (2.6a)$$

$$(\nabla \cdot \check{\mathbf{u}}, \check{q})_{\Omega} = 0 \quad \forall \check{q} \in \check{\mathbb{P}}, \quad (2.6b)$$

$$\langle \check{\mathcal{V}} - \check{\mathbf{u}}, \check{\zeta} \check{\mathbf{n}}_s \rangle_{S(t)} = 0 \quad \forall \check{\zeta} \in L^2(S(t)), \quad (2.6c)$$

$$\langle \mathcal{H} \check{\mathbf{n}}_s, \check{\eta} \rangle_{S(t)} + \langle \nabla_s \text{id}, \nabla_s \check{\eta} \rangle_{S(t)} = 0 \quad \forall \check{\eta} \in [H^1(S(t))]^3. \quad (2.6d)$$

3 Axisymmetric formulations

3.1 The axisymmetric setting

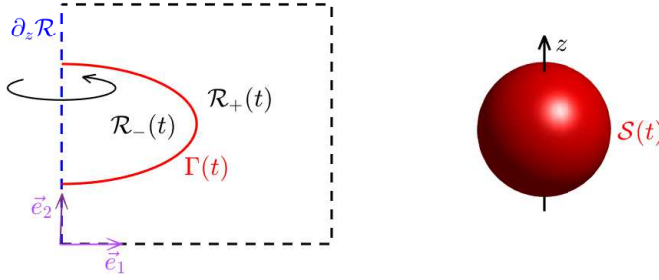


Fig. 1 Left panel: A schematic illustration of the meridian halfplane $\mathcal{R} = \mathcal{R}_-(t) \cup \mathcal{R}_+(t) \cup \Gamma(t)$. Right panel: The axisymmetric surface $S(t)$.

We assume that the considered flow is rotationally symmetric with respect to the z -axis, as shown in Fig. 1. We then start from the 3d formulation (2.6) and derive the axisymmetric weak formulation in the cylindrical coordinates. In this setting, we have the following three assumptions.

- A1** The bounded domain Ω can be obtained by rotating the subset \mathcal{R} of the meridian halfplane with respect to the z -axis. Here $\mathcal{R} = \mathcal{R}_+(t) \cup \mathcal{R}_-(t) \cup \Gamma(t)$, where $\mathcal{R}_{\pm}(t)$ are the corresponding rotated sets for $\Omega_{\pm}(t)$, and $\Gamma(t)$ is the generating curve of the axisymmetric interface $S(t)$.
- A2** We have a natural decomposition of the boundary of \mathcal{R} as $\partial \mathcal{R} = \partial_1 \mathcal{R} \cup \partial_2 \mathcal{R} \cup \partial_z \mathcal{R}$, where $\partial_i \mathcal{R}$ corresponds to $\partial_i \Omega$ for $i = 1, 2$, and $\partial_z \mathcal{R}$ is the artificial boundary of \mathcal{R} .

on the z -axis. Besides, $\Gamma(t)$ is assumed to be a smooth open curve whose two end points are attached to $\partial_z \mathcal{R}$ with a 90° contact angle condition, meaning that $S(t)$ is a smooth genus-0 surface without boundary.

A3 There is no rotational fluid velocity and the velocity components in the r, z -directions are independent of the azimuthal angle φ . Besides, the pressure is independent of φ .

By **A1** and using the cylindrical coordinates, it is natural to consider the following parameterization of the interface $S(t)$

$$\vec{\gamma} : (\alpha, \varphi, t) \mapsto (\bar{x}^r(\alpha, t) \cos \varphi, \bar{x}^z(\alpha, t), \bar{x}^r(\alpha, t) \sin \varphi)^T, \quad \alpha \in \mathbb{I}, \quad \varphi \in [0, 2\pi], \quad (3.1)$$

for $t \in [0, T]$, where $\mathbb{I} = (0, 1)$ with $\partial\mathbb{I} = \{0, 1\}$. Then we could extract the r, z -components to form a parameterization of the generating curve $\Gamma(t)$ as

$$\bar{\mathbf{x}}(\alpha, t) = (\bar{x}^r(\alpha, t), \bar{x}^z(\alpha, t))^T : \mathbb{I} \times [0, T] \rightarrow \mathbb{R}_{\geq 0} \times \mathbb{R}. \quad (3.2)$$

By **A2**, the attachment of the two end points on the z -axis implies that

$$\bar{\mathbf{x}}(\alpha, t) \cdot \vec{e}_1 = 0 \quad \forall \alpha \in \partial\mathbb{I}. \quad (3.3)$$

We further assume that $|\bar{\mathbf{x}}_\alpha(\cdot, t)| > 0$ and $\bar{\mathbf{x}}(\cdot, t) \cdot \vec{e}_1 > 0$ in \mathbb{I} . On introducing the arc length s of the curve $\Gamma(t)$, i.e., $\partial_s = |\bar{\mathbf{x}}_\alpha|^{-1} \partial_\alpha$, the unit tangent and unit normal to the curve $\Gamma(t)$ are defined as

$$\vec{\tau} = \bar{\mathbf{x}}_s, \quad \vec{\nu} = -\vec{\tau}^\perp,$$

where \cdot^\perp denotes a clockwise rotation by $\frac{\pi}{2}$, and $\vec{\nu}$ is the unit normal to Γ and points into $\mathcal{R}_+(t)$. We introduce the mean curvature of $S(t)$,

$$\varkappa = \kappa - \frac{\vec{\nu} \cdot \vec{e}_1}{\bar{\mathbf{x}} \cdot \vec{e}_1} \quad \text{with} \quad \kappa \vec{\nu} = \bar{\mathbf{x}}_{ss}, \quad (3.4)$$

where κ is the curvature of the generating curve $\Gamma(t)$. Clearly, for \varkappa to remain bounded we need that $\vec{\nu} \cdot \vec{e}_1 = 0$ on $\partial\mathbb{I}$, which is equivalent to

$$\vec{\tau} \cdot \vec{e}_2 = 0 \quad \text{on } \partial\mathbb{I}, \quad (3.5)$$

i.e. the 90° contact angle condition from **A2**.

Furthermore, by **A3** we can write the fluid velocity in terms of the cylindrical coordinates as

$$\check{\vec{u}}(\vec{x}, t) = (u^r(r, z, t) \cos \varphi, u^z(r, z, t), u^r(r, z, t) \sin \varphi)^T. \quad (3.6)$$

Then we could extract the r, z components to form a vector field in \mathcal{R} as

$$\vec{u}(r, z, t) = (u^r(r, z, t), u^z(r, z, t))^T : \mathcal{R} \times [0, T] \rightarrow \mathbb{R}^2. \quad (3.7)$$

We further introduce

$$\nabla_c = \vec{e}_1 \partial_r + \vec{e}_2 \partial_z, \quad \underline{\underline{\mathbb{D}}}_c(\vec{u}) = \frac{1}{2}[\nabla_c \vec{u} + (\nabla_c \vec{u})^T]. \quad (3.8)$$

3.2 Axisymmetric weak formulations

By (3.3), we introduce the function space for $\vec{\mathbf{x}}(\cdot, t)$ as

$$V_\partial = \left\{ \vec{\eta} \in [H^1(\mathbb{I})]^2 : \vec{\eta}(\alpha) \cdot \vec{e}_1 = 0 \quad \forall \alpha \in \partial\mathbb{I} \right\}. \quad (3.9)$$

Moreover, we define the weighted Sobolev spaces

$$\begin{aligned} L_a^2(\mathcal{R}) &:= \left\{ \chi : \int_{\mathcal{R}} r^a \chi^2 \, dr dz < +\infty \right\}, \quad a \in \mathbb{R}, \\ H_a^1(\mathcal{R}) &:= \left\{ \chi \in L_a^2(\mathcal{R}) : \partial_r \chi \in L_a^2(\mathcal{R}), \partial_z \chi \in L_a^2(\mathcal{R}) \right\}, \end{aligned}$$

and then introduce the function spaces for the velocity and pressure (see [15, 16])

$$\begin{aligned} \mathbb{U} &:= \left\{ \vec{\chi} \in [H_1^1(\mathcal{R})]^2 : (\vec{\chi} \cdot \vec{e}_1) \in L_{-1}^2(\mathcal{R}), \vec{\chi} = \vec{0} \text{ on } \partial_1 \mathcal{R}, \vec{\chi} \cdot \vec{n} = 0 \text{ on } \partial_2 \mathcal{R} \right\}, \\ \mathbb{V} &:= H^1(0, T; [L_1^2(\mathcal{R})]^2) \cap L^2(0, T; \mathbb{U}), \quad \mathbb{P} := \left\{ \chi \in L_1^2(\mathcal{R}) : \int_{\mathcal{R}} r \chi \, dr dz = 0 \right\}, \end{aligned}$$

where \vec{n} is the outer unit normal to $\partial\mathcal{R}$. Let (\cdot, \cdot) and $\langle \cdot, \cdot \rangle$ be the L^2 -inner products over \mathcal{R} and \mathbb{I} , respectively. Then by imposing the axisymmetric conditions, we are able to transform the 3d formulation (2.6) into a set of equations in the subset \mathcal{R} of the 2d meridian halfplane and in \mathbb{I} as follows. Given the initial velocity $\vec{u}_0 \in \mathbb{U}$ and $\vec{\mathbf{x}}(\cdot, 0) \in V_\partial$, we find $\vec{u} \in \mathbb{V}$, $p \in L^2(0, T; \mathbb{P})$, $\vec{\mathbf{x}} \in H^1(0, T; V_\partial)$ and $\varkappa \in L^2(0, T; L^2(\mathbb{I}))$ such that for all $t \in (0, T]$

$$\begin{aligned} & \frac{1}{2} \left[\frac{d}{dt} (\rho_c \vec{u}, \vec{\chi} r) + (\rho_c \partial_t \vec{u}, \vec{\chi} r) - (\rho_c \vec{u}, \partial_t \vec{\chi} r) \right] + \mathcal{A}(\rho_c, \vec{u}; \vec{u}, \vec{\chi}) \\ & + 2(\mu_c r^{-1} [\vec{u} \cdot \vec{e}_1], \vec{\chi} \cdot \vec{e}_1) + 2(\mu_c r \underline{\underline{D}}_c(\vec{u}), \underline{\underline{D}}_c(\vec{\chi})) - (p, \nabla_c \cdot [r \vec{\chi}]) \\ & - \gamma \langle [\vec{\mathbf{x}} \cdot \vec{e}_1] \varkappa \vec{v}, \vec{\chi} |\vec{\mathbf{x}}_\alpha| \rangle = (\rho_c r \vec{g}, \vec{\chi}) \quad \forall \vec{\chi} \in \mathbb{V}, \end{aligned} \quad (3.11a)$$

$$(\nabla_c \cdot [r \vec{u}], q) = 0 \quad \forall q \in \mathbb{P}, \quad (3.11b)$$

$$\langle (\vec{\mathbf{x}} \cdot \vec{e}_1) [\partial_t \vec{\mathbf{x}} - \vec{u}], \zeta \vec{v} |\vec{\mathbf{x}}_\alpha| \rangle = 0 \quad \forall \zeta \in L^2(\mathbb{I}), \quad (3.11c)$$

$$\langle (\vec{\mathbf{x}} \cdot \vec{e}_1) \varkappa \vec{v}, \vec{\eta} |\vec{\mathbf{x}}_\alpha| \rangle + \langle \vec{e}_1 \cdot \vec{\eta}, |\vec{\mathbf{x}}_\alpha| \rangle + \left\langle \frac{(\vec{\mathbf{x}} \cdot \vec{e}_1)}{|\vec{\mathbf{x}}_\alpha|} \vec{\mathbf{x}}_\alpha, \vec{\eta}_\alpha \right\rangle = 0 \quad \forall \vec{\eta} \in V_\partial, \quad (3.11d)$$

where in these expressions we introduced

$$\rho_c(\cdot, t) = \rho_+ \mathcal{X}_{\mathcal{R}_+(t)} + \rho_- \mathcal{X}_{\mathcal{R}_-(t)}, \quad \mu_c(\cdot, t) = \mu_+ \mathcal{X}_{\mathcal{R}_+(t)} + \mu_- \mathcal{X}_{\mathcal{R}_-(t)}, \quad (3.12a)$$

$$\mathcal{A}(\rho_c, \vec{v}; \vec{u}, \vec{\chi}) = \frac{1}{2} (\rho_c r, [\vec{v} \cdot \nabla_c] \vec{u} \cdot \vec{\chi} - [\vec{v} \cdot \nabla_c] \vec{\chi} \cdot \vec{u}). \quad (3.12b)$$

Compared to (2.6), we note an extra weight r or $\vec{\mathbf{x}} \cdot \vec{e}_1$ was introduced in (3.11) since the volume and surface integrals were transformed into area and line integrals. The detailed derivation of (3.11) is presented in Appendix A. The main advantage of this axisymmetric reduction is that the boundary conditions at the artificial boundary appear naturally in the formulation, see [24]. For example, we actually have the free slip boundary condition for the velocity on $\partial_z \mathcal{R}$, which is inferred by $\vec{u} \in \mathbb{V}$. Moreover,

it can be shown that (3.11d) implies the 90° contact angle condition (3.5), see [13, Appendix A] for details.

In this axisymmetric setting, we denote by $E(\rho_c, \vec{u}(t), \vec{x}(t))$ and $M(\vec{x}(t))$ the energy of the system and the enclosed volume of the axisymmetric surface $S(t)$, respectively. On recalling (2.3) and using (3.1) and (3.6), then it holds

$$E(\rho_c, \vec{u}(t), \vec{x}(t)) = \pi(\rho_c |\vec{u}|^2, r) + 2\pi\gamma \langle \vec{x} \cdot \vec{e}_1, |\vec{x}_\alpha| \rangle, \quad (3.13a)$$

$$M(\vec{x}(t)) = \pi \langle (\vec{x} \cdot \vec{e}_1)^2 \vec{v}, \vec{e}_1 |\vec{x}_\alpha| \rangle, \quad (3.13b)$$

where the reader can refer to [12, (3.10)] for (3.13b). On recalling (2.4) and using direct calculation it is not difficult to show that solutions to (3.11) satisfy

$$\begin{aligned} \frac{d}{dt} E(\vec{u}(t), \vec{x}(t)) &= \pi \frac{d}{dt} (\rho_c |\vec{u}|^2, r) + 2\pi\gamma \langle \vec{x}_t \cdot \vec{e}_1, |\vec{x}_\alpha| \rangle \\ &\quad + 2\pi\gamma \langle \vec{x} \cdot \vec{e}_1, (\vec{x}_t)_\alpha \cdot \vec{x}_\alpha |\vec{x}_\alpha|^{-1} \rangle, \end{aligned} \quad (3.14a)$$

$$\frac{d}{dt} M(\vec{x}(t)) = 2\pi \langle \vec{x} \cdot \vec{e}_1, \vec{x}_t \cdot \vec{v} |\vec{x}_\alpha| \rangle. \quad (3.14b)$$

Now denote

$$\omega(t) = \frac{\int_{\mathcal{R}_{-(t)}} r \, dr dz}{\int_{\mathcal{R}} r \, dr dz}, \quad t \in [0, T]. \quad (3.15)$$

Then it easy to check that $\mathcal{X}_{\mathcal{R}_{-(t)}} - \omega(t) \in \mathbb{P}$. Choosing $q = \mathcal{X}_{\mathcal{R}_{-(t)}} - \omega(t)$ in (3.11b) and $\zeta = 1$ in (3.11c) and using (3.14b) gives rise to

$$\begin{aligned} \frac{d}{dt} M(\vec{x}(t)) &= 2\pi \langle \vec{x} \cdot \vec{e}_1, \vec{x}_t \cdot \vec{v} |\vec{x}_\alpha| \rangle \\ &= 2\pi \langle (\vec{x} \cdot \vec{e}_1) \vec{u} \cdot \vec{v}, |\vec{x}_\alpha| \rangle = 2\pi (\nabla_c \cdot [r \vec{u}], 1) = 0. \end{aligned} \quad (3.16)$$

Moreover, setting $\vec{\chi} = \vec{u}$ in (3.11a), $q = p$ in (3.11b), $\zeta = \gamma\kappa$ in (3.11c) and $\vec{\eta} = \vec{x}_t$ in (3.11d), combining these equations and on recalling (3.14a) yields that

$$\frac{1}{2\pi} \frac{d}{dt} E(\rho_c, \vec{u}(t), \vec{x}(t)) = -2(\mu_c r^{-1} [\vec{u} \cdot \vec{e}_1], [\vec{u} \cdot \vec{e}_1]) - 2(\mu_c r \underline{\underline{D}}_c(\vec{u}), \underline{\underline{D}}_c(\vec{u})) + (\rho_c r \vec{g}, \vec{u}). \quad (3.17)$$

Therefore, we obtain the volume conservation law (3.16) and the energy law (3.17) for the weak solution.

On recalling (3.4), it is also possible to consider an alternative weak formulation, which treats the curvature of the curve $\Gamma(t)$ as an unknown. To this end, let the initial velocity $\vec{u}_0 \in \mathbb{U}$ and the initial generating curve $\vec{x}(\cdot, 0) \in V_\partial$ be given. Then we find $\vec{u} \in \mathbb{V}$, $p \in L^2(0, T; \mathbb{P})$, $\vec{x} \in H^1(0, T; V_\partial)$ and $\kappa \in L^2(0, T; L^2(\mathbb{I}))$ such that for

$t \in (0, T]$

$$\begin{aligned} & \frac{1}{2} \left[\frac{d}{dt} (\rho_c \vec{u}, \vec{\chi} r) + (\rho_c \partial_t \vec{u}, \vec{\chi} r) - (\rho_c \vec{u}, \partial_t \vec{\chi} r) \right] + \mathcal{A}(\rho_c, \vec{u}; \vec{u}, \vec{\chi}) \\ & + 2(\mu_c r^{-1} [\vec{u} \cdot \vec{e}_1], [\vec{\chi} \cdot \vec{e}_1]) + 2(\mu_c r \underline{\underline{D}}_c(\vec{u}), \underline{\underline{D}}_c(\vec{\chi})) - (p, \nabla_c \cdot [r \vec{\chi}]) \\ & - \gamma \langle (\vec{x} \cdot \vec{e}_1) \kappa - \vec{v} \cdot \vec{e}_1, \vec{v} \cdot \vec{\chi} |\vec{x}_\alpha| \rangle = (\rho_c r \vec{g}, \vec{\chi}) \quad \forall \vec{\chi} \in \mathbb{V}, \end{aligned} \quad (3.18a)$$

$$(\nabla_c \cdot [r \vec{u}], q) = 0 \quad \forall q \in \mathbb{P}, \quad (3.18b)$$

$$\langle (\vec{x} \cdot \vec{e}_1) [\partial_t \vec{x} - \vec{u}], \zeta \vec{v} |\vec{x}_\alpha| \rangle = 0 \quad \forall \zeta \in L^2(\mathbb{I}), \quad (3.18c)$$

$$\langle \kappa \vec{v}, \vec{\eta} |\vec{x}_\alpha| \rangle + \langle \vec{x}_\alpha, \vec{\eta}_\alpha |\vec{x}_\alpha|^{-1} \rangle = 0 \quad \forall \vec{\eta} \in V_\partial. \quad (3.18d)$$

Similarly, Choosing $q = \mathcal{X}_{\mathcal{R}_{-(t)}} - \omega(t)$ in (3.18b) and $\zeta = 1$ in (3.18c) then yields that (3.16) is satisfied. Besides, on choosing $\vec{\chi} = \vec{u}$ in (3.18a), $q = p$ in (3.18b), $\zeta = \gamma(\kappa - \frac{\vec{v} \cdot \vec{e}_1}{\vec{x} \cdot \vec{e}_1})$ in (3.18c) and $\vec{\eta} = (\vec{x} \cdot \vec{e}_1) \vec{x}_t$ in (3.18d), we obtain (3.17) as well. The advantage of the weak formulation (3.18) is that it is very close to [11, (3.9)], i.e., to the two-dimensional analogue of (2.6). Moreover, upon discretization this formulation will admit an equidistribution property, thanks to (3.18d). However, we will only be able to prove a stability estimate for discretizations based on the weak formulation (3.11), utilizing techniques developed in [12, 13].

4 Unfitted finite element approximations

We approximate the weak formulations (3.11) and (3.18) for velocity \vec{u} and pressure p on the domain \mathcal{R} , and for the parameterization \vec{x} and the interfaces mean curvature κ , or for the curve's curvature κ , on the reference domain \mathbb{I} using the finite element method. Let $[0, T] = \bigcup_{m=0}^M [t_m, t_{m+1}]$ be a uniform partition of the time domain with $\Delta t = \frac{T}{M}$ and $t_m = m\Delta t$ for $m = 0, 1, \dots, M$.

The reference domain \mathbb{I} is discretized uniformly into $\mathbb{I} = \bigcup_{j=1}^{J_\Gamma} \mathbb{I}_j$ with $\mathbb{I}_j = [\alpha_{j-1}, \alpha_j]$, $\alpha_j = jh$ and $h = 1/J_\Gamma$. We then introduce the finite element spaces

$$V^h := \left\{ \zeta \in C(\bar{\mathbb{I}}) : \zeta|_{\mathbb{I}_j} \text{ is affine } \forall j = 1, \dots, J_\Gamma \right\}, \quad V_\partial^h := [V^h]^2 \cap V_\partial.$$

Let $\{\vec{X}^m\}_{0 \leq m \leq M}$ be an approximation to $\{\vec{x}(t)\}_{t \in [0, T]}$ with $\vec{X}^m \in V_\partial^h$. We define $\Gamma^m = \vec{X}^m(\bar{\mathbb{I}})$, and assume that

$$\vec{X}^m \cdot \vec{e}_1 > 0 \quad \text{in } \bar{\mathbb{I}} \setminus \partial \mathbb{I} \quad \text{and} \quad |\vec{X}_\alpha^m| > 0 \quad \text{in } \mathbb{I}, \quad 0 \leq m \leq M,$$

so that we have the discrete unit tangential and normal vectors

$$\vec{\tau}^m = \vec{X}_s^m = \frac{\vec{X}_\alpha^m}{|\vec{X}_\alpha^m|} \quad \text{and} \quad \vec{\nu}^m = -(\vec{\tau}^m)^\perp.$$

In addition, let $\bar{\mathcal{R}} = \bigcup_{o \in \mathcal{T}^m} \bar{o}$ be a regular partition, where $\mathcal{T}^m := \{o_j^m : j = 1, \dots, J_{\mathcal{R}}^m\}$ are mutually disjoint and non-degenerate triangles. We introduce the finite element spaces associated with the mesh \mathcal{T}^m as

$$\begin{aligned} S_k^m &:= \left\{ \varphi \in C(\bar{\mathcal{R}}) : \varphi|_o \in \mathcal{P}_k(o), \forall o \in \mathcal{T}^m \right\}, \quad k \in \mathbb{N}_+, \\ S_0^m &:= \left\{ \varphi \in L^2(\mathcal{R}) : \varphi|_o \text{ is constant}, \forall o \in \mathcal{T}^m \right\}, \end{aligned}$$

where $\mathcal{P}_k(o)$ denotes the space of polynomials of degree k on o . Let \mathbb{U}^m and \mathbb{P}^m denote the finite element spaces for the numerical solutions of the velocity and pressure, respectively. It is natural to consider the Taylor–Hood pair elements,

$$(\mathbb{U}^m, \mathbb{P}^m) = ([S_2^m]^2 \cap \mathbb{U}, S_1^m \cap \mathbb{P}), \quad (4.1)$$

which guarantees the following inf-sup stability condition for the axisymmetric problem [15, 16]:

$$\inf_{q \in \mathbb{P}^m} \sup_{\vec{\chi} \in \mathbb{U}^m} \frac{(q, \nabla_c \cdot [r\vec{\chi}])}{\|r^{\frac{1}{2}}q\| \|\vec{\chi}\|_*} \geq c > 0. \quad (4.2)$$

Here $\|\cdot\|$ denote the usual L^2 -norm on \mathcal{R} , c is a constant and $\|\cdot\|_*$ is defined as

$$\|\vec{\chi}\|_* = \left(\|r^{\frac{1}{2}}\nabla_c \chi^r\|^2 + \|r^{-\frac{1}{2}}\chi^r\|^2 + \|r^{\frac{1}{2}}\nabla_c \chi^z\|^2 + \|r^{\frac{1}{2}}\chi^z\|^2 \right)^{\frac{1}{2}},$$

for $\vec{\chi} = (\chi^r, \chi^z)^T$.

We consider the unfitted mesh approach, meaning that \mathcal{T}^m may not fit the interface, i.e., the line segments making up Γ^m are in general not the boundaries of elements in \mathcal{T}^m . At $t = t^m$, the interface Γ^m divides \mathcal{R} into two sub-domains \mathcal{R}_-^m and \mathcal{R}_+^m with \mathcal{R}_-^m being the domain enclosed by Γ^m and $\partial_z \mathcal{R}$. We split \mathcal{T}^m into three disjoint subsets \mathcal{T}_-^m , \mathcal{T}_+^m and \mathcal{T}_Γ^m :

$$\mathcal{T}_\pm^m = \{o \in \mathcal{T}^m : o \subset \mathcal{R}_\pm^m\}, \quad \mathcal{T}_\Gamma^m = \{o \in \mathcal{T}^m : o \cap \Gamma^m \neq \emptyset\}.$$

Let ρ^m and μ^m be numerical approximations of the density $\rho_c(\cdot, t)$ and the viscosity $\mu_c(\cdot, t)$ at $t = t_m$, respectively. We define $\rho^m \in S_0^m$ and $\mu^m \in S_0^m$ such that

$$\rho^m|_o := \begin{cases} \rho_-, & \text{if } o \in \mathcal{T}_-^m, \\ \rho_+, & \text{if } o \in \mathcal{T}_+^m, \\ \frac{1}{2}(\rho_- + \rho_+), & \text{if } o \in \mathcal{T}_\Gamma^m, \end{cases} \quad \mu^m|_o := \begin{cases} \mu_-, & \text{if } o \in \mathcal{T}_-^m, \\ \mu_+, & \text{if } o \in \mathcal{T}_+^m, \\ \frac{1}{2}(\mu_- + \mu_+), & \text{if } o \in \mathcal{T}_\Gamma^m. \end{cases}$$

In what follows, we denote by \vec{U}^m , P^m , \varkappa^m , κ^m the numerical approximations of $\vec{u}(\cdot, t)$, $p(\cdot, t)$, $\varkappa(\cdot, t)$ and $\kappa(\cdot, t)$ at time t_m , respectively. Besides, we introduce the standard interpolation operators $I_k^m : C(\bar{\mathcal{R}}) \rightarrow [S_k^m]^2$ for $k \geq 1$, and the standard projection operator $I_0^m : L^1(\mathcal{R}) \rightarrow S_0^m$ with $(I_0^m \eta)|_o = \frac{1}{|o|} \int_o \eta \, r \, dr \, dz$ for $o \in \mathcal{T}^m$. Based on suitable discretizations of the weak formulations (3.11) and (3.18), we next introduce several numerical methods and explore their properties.

4.1 A linear approximation

We start by considering a linear approximation of (3.18). Let $\vec{U}^0 \in \mathbb{U}^0$ be an approximation of the initial velocity \vec{u}_0 . Moreover, the generating curve of the initial interface $\Gamma(0)$ is approximated by a polygonal curve $\Gamma^0 := \vec{X}^0(\mathbb{I})$ with $\vec{X}^0 \in V_\partial$. We set $\rho^{-1} = \rho^0$. Then for $m \geq 0$, we find $\vec{U}^{m+1} \in \mathbb{U}^m$, $P^{m+1} \in \mathbb{P}^m$, $\vec{X}^{m+1} \in V_\partial^h$ and $\kappa^{m+1} \in V^h$ such that it holds

$$\begin{aligned} & \frac{1}{2} \left[\left(\frac{\rho^m \vec{U}^{m+1} - I_0^m \rho^{m-1} I_2^m \vec{U}^m}{\Delta t}, \vec{\chi} r \right) + \left(I_0^m \rho^{m-1} \frac{\vec{U}^{m+1} - I_2^m \vec{U}^m}{\Delta t}, \vec{\chi} r \right) \right] \\ & + \mathcal{A}(\rho^m, I_2^m \vec{U}^m; \vec{U}^{m+1}, \vec{\chi}) + 2(\mu^m \underline{\mathbb{D}}_c(\vec{U}^{m+1}), \underline{\mathbb{D}}_c(\vec{\chi}) r) \\ & + 2(\mu^m r^{-1} [\vec{U}^{m+1} \cdot \vec{e}_1], [\vec{\chi} \cdot \vec{e}_1])^\diamond - (P^{m+1}, \nabla_c \cdot [r \vec{\chi}]) \\ & - \gamma \langle (\vec{X}^m \cdot \vec{e}_1) \kappa^{m+1} - \vec{v}^m \cdot \vec{e}_1, \vec{v}^m \cdot \vec{\chi} |\vec{X}_\alpha^m| \rangle = (\rho^m \vec{g}, \vec{\chi} r), \end{aligned} \quad (4.3a)$$

$$(\nabla_c \cdot [r \vec{U}^{m+1}], q) = 0, \quad (4.3b)$$

$$\frac{1}{\Delta t} \langle (\vec{X}^m \cdot \vec{e}_1) (\vec{X}^{m+1} - \vec{X}^m), \zeta \vec{v}^m |\vec{X}_\alpha^m| \rangle - \langle (\vec{X}^m \cdot \vec{e}_1) \vec{U}^{m+1}, \zeta \vec{v}^m |\vec{X}_\alpha^m| \rangle = 0, \quad (4.3c)$$

$$\langle \kappa^{m+1} \vec{v}^m, \vec{\eta} |\vec{X}_\alpha^m|^h \rangle + \langle \vec{X}_\alpha^{m+1}, \vec{\eta}_\alpha |\vec{X}_\alpha^m|^{-1} \rangle = 0, \quad (4.3d)$$

for all $(\vec{\chi}, q, \zeta, \vec{\eta}) \in \mathbb{U}^m \times \mathbb{P}^m \times V^h \times V_\partial^h$, where $(\cdot, \cdot)^\diamond$ represents an approximation of the inner product (\cdot, \cdot) that ensures that the corresponding term in (4.3a) is well defined for all $\vec{U}^{m+1} \in \mathbb{U}^m$ and $\vec{\chi} \in \mathbb{U}^m$. This is guaranteed by employing quadrature rules with only interior sampling points, such as Gauss–Lobatto quadrature rules. We also introduce $\langle \cdot, \cdot \rangle^h$ as the mass lumped L^2 -inner product over \mathbb{I} . In particular, for two piecewise continuous functions \vec{v}, \vec{w} , with possible jumps at the nodes $\{\alpha_j\}_{j=1}^{J_r}$, it is defined via

$$\langle \vec{v}, \vec{w} \rangle^h = \frac{1}{2} h \sum_{j=1}^{J_r} \left[(\vec{v} \cdot \vec{w})(\alpha_j^-) + (\vec{v} \cdot \vec{w})(\alpha_j^+) \right] \quad \text{with} \quad g(\alpha_j^\pm) = \lim_{\delta \searrow 0} g(\alpha_j \pm \delta).$$

The approximation in (4.3d) leads to an equidistribution property. For a semidiscrete variant this can be made rigorous, while for the fully discrete approximation (4.3) the mesh points on the polygonal curve Γ^m diffuse tangentially towards an equidistant distribution [12]. For a detailed discussion of this equidistribution property, readers are referred to [8, 14].

4.2 An unconditionally stable approximation

We next introduce a suitable discretization of (3.11), which leads to an unconditionally stable finite element method. With the discrete initial data as before, for $m \geq 0$,

we find $\vec{U}^{m+1} \in \mathbb{U}^m$, $\mathbf{P}^{m+1} \in \mathbb{P}^m$, $\vec{X}^{m+1} \in V_\partial^h$ and $\varkappa^{m+1} \in V^h$ such that it holds

$$\begin{aligned} & \frac{1}{2} \left[\left(\frac{\rho^m \vec{U}^{m+1} - I_0^m \rho^{m-1} I_2^m \vec{U}^m}{\Delta t}, \vec{\chi} r \right) + \left(I_0^m \rho^{m-1} \frac{\vec{U}^{m+1} - I_2^m \vec{U}^m}{\Delta t}, \vec{\chi} r \right) \right] \\ & + \mathcal{A}(\rho^m, I_2^m \vec{U}^m; \vec{U}^{m+1}, \vec{\chi}) + 2(\mu^m \underline{\mathbb{D}}_c(\vec{U}^{m+1}), \underline{\mathbb{D}}_c(\vec{\chi}) r) \\ & + 2(\mu^m r^{-1} [\vec{U}^{m+1} \cdot \vec{e}_1], [\vec{\chi} \cdot \vec{e}_1])^\circ - (\mathbf{P}^{m+1}, \nabla_c \cdot [r \vec{\chi}]) \\ & - \gamma \langle (\vec{X}^m \cdot \vec{e}_1) \varkappa^{m+1} \vec{v}^m, \vec{\chi} |\vec{X}_\alpha^m| \rangle = (\rho^m \vec{g}, \vec{\chi} r), \end{aligned} \quad (4.4a)$$

$$(\nabla_c \cdot [r \vec{U}^{m+1}], q) = 0, \quad (4.4b)$$

$$\frac{1}{\Delta t} \langle (\vec{X}^m \cdot \vec{e}_1) (\vec{X}^{m+1} - \vec{X}^m), \zeta \vec{v}^m |\vec{X}_\alpha^m| \rangle - \langle (\vec{X}^m \cdot \vec{e}_1) \vec{U}^{m+1}, \zeta \vec{v}^m |\vec{X}_\alpha^m| \rangle = 0, \quad (4.4c)$$

$$\langle (\vec{X}^m \cdot \vec{e}_1) \varkappa^{m+1} \vec{v}^m, \vec{\eta} |\vec{X}_\alpha^m| \rangle + \langle \vec{\eta} \cdot \vec{e}_1, |\vec{X}_\alpha^{m+1}| \rangle + \langle (\vec{X}^m \cdot \vec{e}_1) \vec{X}_\alpha^{m+1}, \vec{\eta}_\alpha |\vec{X}_\alpha^m|^{-1} \rangle = 0, \quad (4.4d)$$

for all $(\vec{\chi}, q, \zeta, \vec{\eta}) \in \mathbb{U}^m \times \mathbb{P}^m \times V^h \times V_\partial^h$. Observe that the only differences with respect to (4.3) are (4.4d) and the final term on the left hand side of (4.4a). In addition, we note that (4.4) leads to a system of nonlinear equations due to the presence of $|\vec{X}_\alpha^{m+1}|$ in the second term of (4.4d). This particular nonlinear approximation contributes to the stability of the interface energy, see [12]. We have the following theorem for the introduced method (4.4), which mimics (3.17) on the discrete level.

Theorem 4.1 *Let $(\vec{U}^{m+1}, \mathbf{P}^{m+1}, \vec{X}^{m+1}, \varkappa^{m+1})$ be a solution of (4.4). Then it holds that*

$$\begin{aligned} & \frac{1}{2\pi} E(\rho^m, \vec{U}^{m+1}, \vec{X}^{m+1}) + 2\Delta t \left(\|\sqrt{\mu^m} r \underline{\mathbb{D}}_c(\vec{U}^{m+1})\|^2 + \|\sqrt{\mu^m} r^{-1} [\vec{U}^{m+1} \cdot \vec{e}_1]\|_\diamond^2 \right) \\ & \leq \frac{1}{2\pi} E(I_0^m \rho^{m-1}, I_2^m \vec{U}^m, \vec{X}^m) + \Delta t (\rho^m r \vec{g}, \vec{U}^{m+1}), \quad m = 0, \dots, M-1, \end{aligned} \quad (4.5)$$

where $\|\cdot\|$ and $\|\cdot\|_\diamond$ are the induced norms of the inner products (\cdot, \cdot) and $(\cdot, \cdot)^\circ$, respectively. Moreover, on assuming that

$$E(I_0^m \rho^{m-1}, I_2^m \vec{U}^m, \vec{X}^m) \leq E(\rho^{m-1}, \vec{U}^m, \vec{X}^m), \quad \text{for } m = 0, \dots, M-1, \quad (4.6)$$

it holds that for $k = 0, \dots, M-1$.

$$\begin{aligned} & \frac{1}{2\pi} E(\rho^k, \vec{U}^{k+1}, \vec{X}^{k+1}) + 2\Delta t \sum_{m=0}^k \left\{ \|\sqrt{\mu^m} r \underline{\mathbb{D}}_c(\vec{U}^{m+1})\|^2 + \|\sqrt{\mu^m} r^{-1} [\vec{U}^{m+1} \cdot \vec{e}_1]\|_\diamond^2 \right\} \\ & \leq \frac{1}{2\pi} E(\rho^0, \vec{U}^0, \vec{X}^0) + \Delta t \sum_{m=0}^k (\rho^m r \vec{g}, \vec{U}^{m+1}). \end{aligned} \quad (4.7)$$

Proof Setting $\vec{\chi} = \Delta t \vec{U}^{m+1}$ in (4.4a), $q = P^{m+1}$ in (4.4b), $\zeta = \Delta t \gamma \kappa^{m+1}$ in (4.4c) and $\vec{\eta} = \vec{X}^{m+1} - \vec{X}^m$ in (4.4d), and combining these equations yields that

$$\begin{aligned} & \frac{1}{2} \left(\rho^m \vec{U}^{m+1} - I_0^m \rho^{m-1} I_2^m \vec{U}^m + I_0^m \rho^{m-1} [\vec{U}^{m+1} - I_2^m \vec{U}^m], \vec{U}^{m+1} r \right) \\ & + 2\Delta t (\mu^m r \underline{\mathbb{D}}_c(\vec{U}^{m+1}), \underline{\mathbb{D}}_c(\vec{U}^{m+1})) + 2\Delta t (\mu^m r^{-1} [\vec{U}^{m+1} \cdot \vec{e}_1], [\vec{U}^{m+1} \cdot \vec{e}_1])^\diamond \\ & + \gamma \langle (\vec{X}^{m+1} - \vec{X}^m) \cdot \vec{e}_1, |\vec{X}_\alpha^{m+1}| \rangle + \gamma \langle (\vec{X}^m \cdot \vec{e}_1) \vec{X}_\alpha^{m+1}, (\vec{X}^{m+1} - \vec{X}^m)_\alpha |\vec{X}_\alpha^m|^{-1} \rangle \\ & = (\rho^m r \vec{g}, \vec{U}^{m+1}). \end{aligned} \quad (4.8)$$

It is straightforward to show that the following equation holds

$$\begin{aligned} & (\rho^m \vec{U}^{m+1} - I_0^m \rho^{m-1} I_2^m \vec{U}^m + I_0^m \rho^{m-1} [\vec{U}^{m+1} - I_2^m \vec{U}^m], \vec{U}^{m+1} r) \\ & = (\rho^m \vec{U}^{m+1}, \vec{U}^{m+1} r) - (I_0^m \rho^{m-1} I_2^m \vec{U}^m, I_2^m \vec{U}^m r) \\ & \quad + (I_0^m \rho^{m-1} [\vec{U}^{m+1} - I_2^m \vec{U}^m], [\vec{U}^{m+1} - I_2^m \vec{U}^m] r) \\ & \geq (\rho^m \vec{U}^{m+1}, \vec{U}^{m+1} r) - (I_0^m \rho^{m-1} I_2^m \vec{U}^m, I_2^m \vec{U}^m r). \end{aligned} \quad (4.9)$$

Moreover, using the inequality $\vec{a} \cdot (\vec{a} - \vec{b}) \geq |\vec{b}|(|\vec{a}| - |\vec{b}|)$ for $\vec{a}, \vec{b} \in \mathbb{R}^2$, we have

$$\begin{aligned} & \langle (\vec{X}^{m+1} - \vec{X}^m) \cdot \vec{e}_1, |\vec{X}_\alpha^{m+1}| \rangle + \langle (\vec{X}^m \cdot \vec{e}_1) \vec{X}_\alpha^{m+1}, (\vec{X}^{m+1} - \vec{X}^m)_\alpha |\vec{X}_\alpha^m|^{-1} \rangle \\ & \geq \langle (\vec{X}^{m+1} - \vec{X}^m) \cdot \vec{e}_1, |\vec{X}_\alpha^{m+1}| \rangle + \langle \vec{X}^m \cdot \vec{e}_1, |\vec{X}_\alpha^{m+1}| - |\vec{X}_\alpha^m| \rangle \\ & = \langle \vec{X}^{m+1} \cdot \vec{e}_1, |\vec{X}_\alpha^{m+1}| \rangle - \langle \vec{X}^m \cdot \vec{e}_1, |\vec{X}_\alpha^m| \rangle. \end{aligned} \quad (4.10)$$

Inserting (4.9) and (4.10) into (4.8), and using (3.13a), we obtain (4.5) as claimed. Summing (4.5) for $m = 0, \dots, k$ and recalling (4.6) yields (4.7).

4.3 Volume-preserving approximations

We recall from §3 that on the continuous level the volume preservation property (3.16) holds for the two axisymmetric weak formulations (3.11) and (3.18). However, the two schemes (4.3) and (4.4) will in general not conserve the volume of the two phases. In order to motivate a remedy, we first consider the semidiscrete setting, following similar considerations in [10, 11]. In particular, the semidiscrete variant of (3.11b) and (3.11c) reads

$$(\nabla_c \cdot [r \vec{u}^h], q^h) = 0 \quad \forall q^h \in \mathbb{P}^h, \quad (4.11a)$$

$$\langle (\vec{x}^h \cdot \vec{e}_1) [\partial_t \vec{x}^h - \vec{u}^h], \zeta^h \vec{v}^h |\vec{x}_\alpha| \rangle = 0 \quad \forall \zeta \in V^h, \quad (4.11b)$$

where we use the superscript h to denote the corresponding quantities on the semidiscrete level. In a similar manner to (3.16), and on choosing suitable test functions, it is not difficult to prove that

$$\frac{d}{dt} M(\vec{x}^h(t)) = 2\pi \langle \vec{x}^h \cdot \vec{e}_1, \vec{x}_t^h \cdot \vec{v}^h |\vec{x}_\alpha| \rangle = 0 \quad (4.12)$$

if the following condition holds

$$\mathcal{X}_{\mathcal{R}_{\underline{h}}^h(t)} - \omega^h(t) \in \mathbb{P}^h \quad \text{with} \quad \omega^h(t) = \frac{\int_{\mathcal{R}_{\underline{h}}^h(t)} r \, dr dz}{\int_{\mathcal{R}} r \, dr dz}, \quad t \in [0, T]. \quad (4.13)$$

This suggest to enrich the discrete pressure spaces \mathbb{P}^h with the single extra function in (4.13). On the fully discrete level this corresponds to ensuring that

$$\mathcal{X}_{\mathcal{R}_{\underline{m}}^m} - \omega^m \in \mathbb{P}^m \quad \text{with} \quad \omega^m = \frac{\int_{\mathcal{R}_{\underline{m}}^m} r \, dr dz}{\int_{\mathcal{R}} r \, dr dz}, \quad m = 0, \dots, M-1. \quad (4.14)$$

Therefore we enforce this by adding the single basis function $\mathcal{X}_{\mathcal{R}_{\underline{m}}^m} - \omega^m$ to the discrete pressure space \mathbb{P}^m , a procedure which we call XFEM. The contribution of this new basis function to (4.3a), (4.3b), (4.4a) and (4.4b) can be rewritten in terms of integrals over \mathbb{I} , on noting that

$$(\nabla_c \cdot [r \vec{\chi}], \mathcal{X}_{\mathcal{R}_{\underline{m}}^m}) = \int_{\mathcal{R}_{\underline{m}}^m} \nabla_c \cdot [r \vec{\chi}] \, dr dz = \langle (\vec{X}^m \cdot \vec{e}_1) \vec{\chi}, \vec{v}^m \rangle \quad \forall \vec{\chi} \in \mathbb{U}^m. \quad (4.15)$$

We note that this XFEM technique was first introduced for the discretizations of (2.6) in [11], leading to good volume conservation in practice. Nevertheless, in order to satisfy an exact volume preservation also on the fully discrete level, it turns out that suitable time-weighted approximations of the interface normals are needed, see [6, 7].

We follow the idea in [6] and introduce $\vec{f}^{m+\frac{1}{2}}$ as an appropriate approximation of the quantity $\vec{f} = \vec{x} \cdot \vec{e}_1 |\vec{x}_\alpha| \vec{v}$. Precisely, we define $\vec{f}^{m+\frac{1}{2}} \in [L^\infty(\mathbb{I})]^2$ by

$$\vec{f}^{m+\frac{1}{2}} = -\frac{1}{6} [(\vec{X}^m \cdot \vec{e}_1) \vec{X}_\alpha^m + 4(\vec{X}^{m+\frac{1}{2}} \cdot \vec{e}_1) \vec{X}_\alpha^{m+\frac{1}{2}} + (\vec{X}^{m+1} \cdot \vec{e}_1) \vec{X}_\alpha^{m+1}]^\perp, \quad (4.16)$$

where $\vec{X}^{m+\frac{1}{2}} = \frac{1}{2}(\vec{X}^m + \vec{X}^{m+1})$. Then we have the following result from [6, Lemma 3.1]. For the sake of completeness, we include the proof here as well.

Lemma 4.1 *Let $\vec{X}^m \in V_\partial^h$ and $\vec{X}^{m+1} \in V_\partial^h$. Then it holds that*

$$M(\vec{X}^{m+1}) - M(\vec{X}^m) = 2\pi \langle \vec{X}^{m+1} - \vec{X}^m, \vec{f}^{m+\frac{1}{2}} \rangle. \quad (4.17)$$

Proof We first introduce a linear approximation in time between \vec{X}^m and \vec{X}^{m+1} as

$$\vec{X}^h(t) := \frac{t_{m+1} - t}{\Delta t} \vec{X}^{m+1} + \frac{t - t_m}{\Delta t} \vec{X}^m \in V_\partial^h, \quad t \in [t_m, t_{m+1}]. \quad (4.18)$$

Then applying (3.14b) to $\vec{X}^h(t)$ yields that

$$\frac{d}{dt} M(\vec{X}^h(t)) = 2\pi \langle \vec{X}^h \cdot \vec{e}_1, \vec{X}_t^h \cdot \vec{v}^h |\vec{X}_\alpha^h| \rangle \quad \forall t \in (t_m, t_{m+1}). \quad (4.19)$$

Integrating (4.19) from t_m to t_{m+1} , and noting that $\vec{X}_t^h = \frac{\vec{X}^{m+1} - \vec{X}^m}{\Delta t}$ and $\vec{v}^h = -\frac{(\vec{X}_\alpha^h)^\perp}{|\vec{X}_\alpha^h|}$, yields that

$$\begin{aligned} M(\vec{X}^{m+1}) - M(\vec{X}^m) &= 2\pi \int_{t_m}^{t_{m+1}} \int_{\mathbb{I}} (\vec{X}^h \cdot \vec{e}_1) \frac{\vec{X}^{m+1} - \vec{X}^m}{\Delta t} \cdot (-\vec{X}_\alpha^h)^\perp \, d\alpha \, dt \\ &= 2\pi \int_{\mathbb{I}} \frac{\vec{X}^{m+1} - \vec{X}^m}{\Delta t} \cdot \int_{t_m}^{t_{m+1}} (\vec{X}^h \cdot \vec{e}_1) (-\vec{X}_\alpha^h)^\perp \, dt \, d\alpha \\ &= 2\pi \int_{\mathbb{I}} (\vec{X}^{m+1} - \vec{X}^m) \cdot \vec{f}^{m+\frac{1}{2}} \, d\alpha, \end{aligned}$$

where in the last equality we employed Simpson's rule on noting that the integrand $(\vec{X}^h \cdot \vec{e}_1) (-\vec{X}_\alpha^h)^\perp$ is a quadratic function in t .

We are now in a position to adapt the numerical method (4.4) to yield an exactly volume conserving scheme as follows. For $m \geq 0$, we find $\vec{U}^{m+1} \in \mathbb{U}^m$, $\mathbf{P}^{m+1} \in \mathbb{P}^m$, $\vec{X}^{m+1} \in V_\theta^h$ and $\kappa^{m+1} \in V^h$ such that it holds

$$\begin{aligned} \frac{1}{2} & \left[\left(\frac{\rho^m \vec{U}^{m+1} - I_0^m \rho^{m-1} I_2^m \vec{U}^m}{\Delta t}, \vec{\chi} \, r \right) + \left(I_0^m \rho^{m-1} \frac{\vec{U}^{m+1} - I_2^m \vec{U}^m}{\Delta t}, \vec{\chi} \, r \right) \right] \\ & + \mathcal{A}(\rho^m, I_2^m \vec{U}^m; \vec{U}^{m+1}, \vec{\chi}) + 2(\mu^m \underline{\mathbb{D}}_c(\vec{U}^{m+1}), \underline{\mathbb{D}}_c(\vec{\chi}) \, r) \\ & + 2(\mu^m r^{-1} [\vec{U}^{m+1} \cdot \vec{e}_1], [\vec{\chi} \cdot \vec{e}_1]^\circ) - (\mathbf{P}^{m+1}, \nabla_c \cdot [r \vec{\chi}]) \\ & - \gamma \langle (\vec{X}^m \cdot \vec{e}_1) \kappa^{m+1}, \vec{v}^m \cdot \vec{\chi} |\vec{X}_\alpha^m| \rangle = (\rho^m \vec{g}, \vec{\chi} \, r), \end{aligned} \quad (4.20a)$$

$$(\nabla_c \cdot [r \vec{U}^{m+1}], q) = 0, \quad (4.20b)$$

$$\frac{1}{\Delta t} \langle \vec{X}^{m+1} - \vec{X}^m, \zeta \vec{f}^{m+\frac{1}{2}} \rangle - \langle (\vec{X}^m \cdot \vec{e}_1) \vec{U}^{m+1}, \zeta \vec{v}^m |\vec{X}_\alpha^m| \rangle = 0, \quad (4.20c)$$

$$\langle \kappa^{m+1} \vec{f}^{m+\frac{1}{2}}, \vec{\eta} \rangle + \langle \vec{\eta} \cdot \vec{e}_1, |\vec{X}_\alpha^{m+1}| \rangle + \langle (\vec{X}^m \cdot \vec{e}_1) \vec{X}_\alpha^{m+1}, \vec{\eta}_\alpha |\vec{X}_\alpha^m|^{-1} \rangle = 0, \quad (4.20d)$$

for all $(\vec{\chi}, q, \zeta, \vec{\eta}) \in \mathbb{U}^m \times \mathbb{P}^m \times V^h \times V_\theta^h$. Here in (4.20c), we employ a semi-implicit treatment $\vec{f}^{m+\frac{1}{2}}$ to approximate $(\vec{x} \cdot \vec{e}_1) |\vec{x}_\alpha| \vec{v}$ instead of the explicit treatment in (4.4c). This then enables the exact volume preservation. Besides, we also employ $\vec{f}^{m+\frac{1}{2}}$ in (4.20d) in order to maintain our stability bound. We then have the following theorem for the scheme (4.20), which mimics (3.16) and (3.17) on the discrete level.

Theorem 4.2 *Let $(\vec{U}^{m+1}, \mathbf{P}^{m+1}, \vec{X}^{m+1}, \kappa^{m+1})$ be a solution of (4.20). Then (4.5) holds. If the condition (4.6) is satisfied, then (4.7) holds for $k = 0, \dots, M-1$. Moreover, if (4.14) holds then*

$$M(\vec{X}^{m+1}) = M(\vec{X}^m), \quad m = 0, \dots, M-1. \quad (4.21)$$

Proof The stability results can be shown as in the proof of Theorem 4.1. For the volume preservation, we choose $q = (\mathcal{X}_{\vec{r}^m} - \omega^m) \in \mathbb{P}^m$ in (4.20b) and obtain

$$(\nabla_c \cdot [r \vec{U}^{m+1}], \mathcal{X}_{\vec{r}^m}) - \omega^m (\nabla_c \cdot [r \vec{U}^{m+1}], 1) = 0. \quad (4.22)$$

Using integration by parts, we can recast (4.22) as

$$\begin{aligned} 0 &= (\nabla_c \cdot [r \vec{U}^{m+1}], \mathcal{X}_{\mathcal{R}^m}) - \omega^m (\nabla_c \cdot [r \vec{U}^{m+1}], 1) \\ &= \int_{\Gamma^m} (\vec{X}^m \cdot \vec{e}_1) \vec{U}^{m+1} \cdot \vec{\nu}^m \, ds = \langle (\vec{X}^m \cdot \vec{e}_1) \vec{U}^{m+1}, \vec{\nu}^m |\vec{X}_\alpha^m| \rangle. \end{aligned} \quad (4.23)$$

On the other hand, setting $\zeta = \Delta t$ in (4.20c) and using (4.23) we obtain

$$\langle \vec{X}^{m+1} - \vec{X}^m, \vec{f}^{m+\frac{1}{2}} \rangle = \Delta t \langle (\vec{X}^m \cdot \vec{e}_1) \vec{U}^{m+1}, \vec{\nu}^m |\vec{X}_\alpha^m| \rangle = 0, \quad (4.24)$$

which implies the desired volume preservation (4.21) on recalling Lemma 4.1.

It is not difficult to also adapt the linear scheme (4.3) into an exactly volume preserving method. In fact, the new scheme, which is now nonlinear, is given by (4.3) with (4.3c) replaced by (4.20c).

Theorem 4.3 *Let $(\vec{U}^{m+1}, P^{m+1}, \vec{X}^{m+1}, \kappa^{m+1})$ be a solution of the adapted scheme (4.3) with (4.3c) replaced by (4.20c). On assuming that (4.14) is satisfied, it holds that*

$$M(\vec{X}^{m+1}) = M(\vec{X}^m), \quad m = 0, \dots, M-1. \quad (4.25)$$

Proof The proof is exactly the same as that of (4.21).

4.4 Nonlinear solvers

We note that apart from (4.3), all our introduced schemes lead to systems of nonlinear equations at each time step. The linear systems arising from (4.3) can be solved with the help of a Schur complement approach and preconditioned Krylov iterative solvers, as described in [11]. For the nonlinear systems resulting from the other schemes, we employ a Picard-type iteration. For example, in order to solve for (4.20), we first set the initial guess $\vec{X}^{m+1,0} = \vec{X}^m$. Then, for each $l \geq 0$, we find $(\vec{U}^{m+1,l+1}, P^{m+1,l+1}, \vec{X}^{m+1,l+1}, \chi^{m+1,l+1}) \in \mathbb{U}^m \times \mathbb{P}^m \times V_\partial^h \times V^h$ such that it holds

$$\begin{aligned} \frac{1}{2} & \left[\left(\frac{\rho^m \vec{U}^{m+1,l+1} - I_0^m \rho^{m-1} I_2^m \vec{U}^m}{\Delta t}, \vec{\chi} r \right) + \left(I_0^m \rho^{m-1} \frac{\vec{U}^{m+1,l+1} - I_2^m \vec{U}^m}{\Delta t}, \vec{\chi} r \right) \right] \\ & + \mathcal{A}(\rho^m, I_2^m \vec{U}^m; \vec{U}^{m+1,l+1}, \vec{\chi}) + 2(\mu^m \underline{\mathbb{D}}_c(\vec{U}^{m+1,l+1}), \underline{\mathbb{D}}_c(\vec{\chi}) r) \\ & + 2(\mu^m r^{-1} [\vec{U}^{m+1,l+1} \cdot \vec{e}_1], [\vec{\chi} \cdot \vec{e}_1])^\diamond - (P^{m+1,l+1}, \nabla_c \cdot [r \vec{\chi}]) \\ & - \gamma \langle (\vec{X}^m \cdot \vec{e}_1) \chi^{m+1,l+1} \vec{\nu}^m, \vec{\chi} |\vec{X}_\alpha^m| \rangle = (\rho^m \vec{g}, \vec{\chi} r), \end{aligned} \quad (4.26a)$$

$$(\nabla_c \cdot [r \vec{U}^{m+1,l+1}], q) = 0, \quad (4.26b)$$

$$\frac{1}{\Delta t} \langle \vec{X}^{m+1,l+1} - \vec{X}^m, \zeta \vec{f}^{m+\frac{1}{2},l} \rangle - \langle (\vec{X}^m \cdot \vec{e}_1) \vec{U}^{m+1,l+1}, \zeta \vec{\nu}^m |\vec{X}_\alpha^m| \rangle = 0, \quad (4.26c)$$

$$\langle \chi^{m+1,l+1} \vec{f}^{m+\frac{1}{2},l}, \vec{\eta} \rangle + \langle \vec{\eta} \cdot \vec{e}_1, |\vec{X}_\alpha^{m+1,l}| \rangle + \langle (\vec{X}^m \cdot \vec{e}_1) \vec{X}_\alpha^{m+1,l+1}, \vec{\eta}_\alpha |\vec{X}_\alpha^m|^{-1} \rangle = 0, \quad (4.26d)$$

for all $(\vec{x}, q, \zeta, \vec{\eta}) \in \mathbb{U}^m \times \mathbb{P}^m \times V^h \times V_{\partial}^h$, where $f^{m+\frac{1}{2},l}$ is a lagged approximation which follows (4.16) directly except that \vec{X}^{m+1} was replaced by $\vec{X}^{m+1,l}$. The system (4.26) is linear and of the same general structure as (4.3). Hence it can be efficiently solved with the aforementioned solution techniques. We repeat the above iteration until

$$\max_{0 \leq j \leq J_f} \left| \vec{X}^{m+1,l+1}(\alpha_j) - \vec{X}^{m+1,l}(\alpha_j) \right| \leq \text{tol}, \quad (4.27)$$

where tol is a chosen tolerance.

5 Numerical results

We implemented our unfitted finite element approximations within the finite element toolbox Alberta, [49]. For the quadrature $(\cdot, \cdot)^\diamond$ we employ a Gauss–Lobatto formula that is exact for polynomials up to degree 17. For the velocity and pressure approximation in the bulk we always use the lowest order Taylor–Hood element, together with our XFEM extension of the pressure space, recall (4.1) and §4.3.

As pointed out in [24, p. 125], it is often quite straightforward to extend existing 2d finite element codes to the axisymmetric setting. For example, we use the same adaptive mesh strategies as in [11] that lead to locally refined bulk meshes close to the interface. For the specification of the mesh parameters we use the same notation as there: $nadapt_{k,l}$ means the time step size is set to $\Delta t = 10^{-3}/n$, the discrete interface is partitioned into $J_f = 2^k$ elements and the two bulk mesh refinement parameters $N_f = 2^k$ and $N_c = 2^l$ indicate the mesh sizes employed close to the interface and far away from it, respectively. We refer to [11] for a more detailed description of the adaptive mesh refinement strategies. For simplicity, we denote the introduced methods (4.4) and (4.20) by Stab^h and $\text{Stab}V^h$, respectively. Moreover, we use Equid^h to denote the method (4.3), and $\text{Equid}V^h$ to denote the scheme (4.3) with (4.3c) replaced by (4.20c).

5.1 The rising bubble

Inspired by the 2d benchmark computations proposed in [36], see [11] for their generalizations to 3d, we study the dynamics of a rising bubble in a bounded cylinder of diameter 1 and height 2. The initial interface of the bubble is given by a sphere of radius $\frac{1}{4}$ and centre $(0, 0, \frac{1}{2})^T$. This means that in cylindrical coordinates, we have $\mathcal{R} = [0, \frac{1}{2}] \times [0, 2]$ and $\Gamma(0) = \{\vec{x} \in \mathcal{R} : |\vec{x} - (0, \frac{1}{2})^T| = \frac{1}{4}\}$. In order to monitor the progress of the rising bubble, we introduce the discrete benchmark quantities

$$\begin{aligned} \delta|_{t_m} &:= \left(\frac{9}{2\pi^2} \right)^{\frac{1}{3}} \frac{[M(\vec{X}^m)]^{\frac{2}{3}}}{\int_0^1 (\vec{X}^m \cdot \vec{e}_1) |\vec{X}_\alpha^m| \, d\alpha}, & V_c|_{t_m} &:= \frac{2\pi \int_{\mathcal{R}^m} (\vec{U}^m \cdot \vec{e}_2) r \, dr dz}{M(\vec{X}^m)}, \\ z_c|_{t_m} &:= \frac{2\pi \int_{\mathcal{R}^m} (\text{id} \cdot \vec{e}_2) r \, dr dz}{M(\vec{X}^m)}, & v_\Delta|_{t_m} &:= \frac{M(\vec{X}^m) - M(\vec{X}^0)}{M(\vec{X}^0)}, \end{aligned}$$

Table 1 Benchmark quantities of the rising bubble in case I.

	Stab ^h			StabV ^h		
	adapt _{5,3}	adapt _{7,3}	2adapt _{9,4}	adapt _{5,3}	adapt _{7,3}	2adapt _{9,4}
β_{\min}	0.9630	0.9536	0.9501	0.9630	0.9536	0.9501
$t_{\beta=\beta_{\min}}$	3.000	2.9960	3.0000	3.000	3.0000	3.0000
$V_{c,\max}$	0.3687	0.3637	0.3642	0.3686	0.3640	0.3643
$t_{V_c=V_{c,\max}}$	1.233	0.8950	0.9255	1.233	0.8980	0.9255
$z_c(t=3)$	1.4834	1.4848	1.4897	1.4835	1.4848	1.4897
$v_A(t=3)$	8.50E-5	-8.27E-5	-2.83E-5	0	0	0

	Equid ^h			EquidV ^h		
	adapt _{5,2}	adapt _{7,3}	2adapt _{9,4}	adapt _{5,2}	adapt _{7,3}	2adapt _{9,4}
β_{\min}	0.9603	0.9534	0.9501	0.9603	0.9534	0.9501
$t_{\beta=\beta_{\min}}$	3.0000	3.0000	3.0000	3.0000	3.0000	3.0000
$V_{c,\max}$	0.3681	0.3637	0.3642	0.3683	0.3637	0.3642
$t_{V_c=V_{c,\max}}$	1.236	0.8980	0.9260	1.236	0.8980	0.9260
$z_c(t=3)$	1.4815	1.4846	1.4896	1.4815	1.4846	1.4896
$v_A(t=3)$	-4.39E-5	-4.58E-5	-2.54E-5	0	0	0

where β denotes the degree of sphericity of the bubble, V_c is the bubble's rise velocity, z_c is the bubble's centre of mass in the vertical direction, v_A is the relative volume loss.

We consider two difference cases, and the physical parameters are given as in [36], see also [11].

– Case I:

$$\rho_+ = 1000, \quad \rho_- = 100, \quad \mu_+ = 10, \quad \mu_- = 1, \quad \gamma = 24.5, \quad \vec{g} = (0, -0.98)^T.$$

– Case II:

$$\rho_+ = 1000, \quad \rho_- = 1, \quad \mu_+ = 10, \quad \mu_- = 0.1, \quad \gamma = 1.96, \quad \vec{g} = (0, -0.98)^T.$$

We first consider case I and use the P2-P1 pair elements in (4.1) with XFEM that discussed in §4.3 to improve the volume preservation. The benchmark results computed by the four introduced methods are reported in Table 1. We observe that these methods can produce quite similar results, and the volume of the bubble is well preserved. In particular, we observe the exact volume preservation for StabV^h and EquidV^h, which numerically verifies (4.21) and (4.25). To examine the quality of the interface mesh, we introduce the mesh ratio function

$$r_h|_{t_m} = \frac{\max_{1 \leq j \leq J_I} |\vec{X}^m(\alpha_j) - \vec{X}^m(\alpha_{j-1})|}{\min_{1 \leq j \leq J_I} |\vec{X}^m(\alpha_j) - \vec{X}^m(\alpha_{j-1})|}, \quad (5.2)$$

and plot the time history of r_h in Fig. 2. We find that for both the methods StabV^h and EquidV^h, the value of the mesh ratio function will in general not exceed 2.0 for $t \leq 3$. This implies the good mesh quality. For the experiment using the method EquidV^h with 2adapt_{9,4}, several snapshots of the generating curves are shown in Fig. 3. Moreover, in Fig. 3 we visualise the computational mesh and the bubble at the final time $t = 3$. Plots of the benchmark quantities versus time are shown as well in Fig. 3.

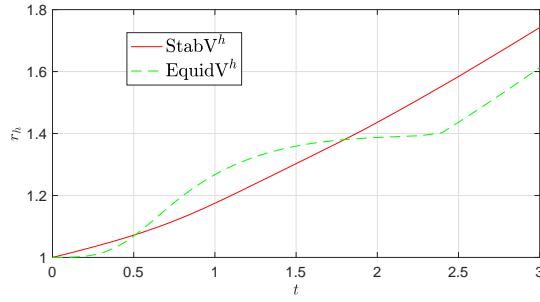


Fig. 2 The time history of the mesh ratio function r_h defined in (5.2) for the methods StabV^h and EquidV^h with $2\text{adapt}_{9,4}$.

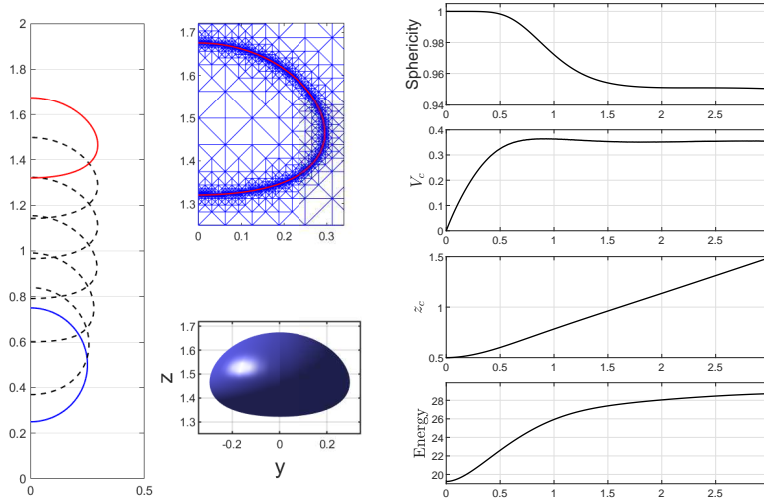


Fig. 3 Evolution of the rising bubble in case I using the method EquidV^h with $2\text{adapt}_{9,4}$. On the left we show the generating curves of the interfaces at $t = 0, 0.5, \dots, 3$ with visualisations of the computational mesh and the axisymmetric surface $S(t)$ at the final time $t = 3$. On the right are plots of the discrete benchmark quantities versus time.

We next consider the rising bubble problem in case II. In this case, the rising bubble can exhibit strong deformations due to the high density ratio and viscosity ratio. The benchmark results are reported in Table 2. For the experiment using the method StabV^h with $2\text{adapt}_{9,4}$, we show the evolving interfaces and the plots of the benchmark results in Fig. 4 and Fig. 5, respectively.

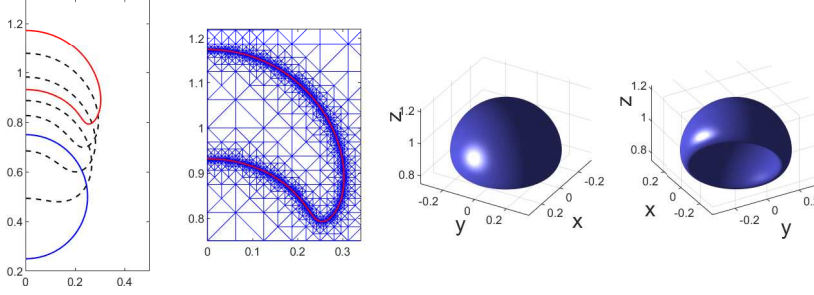
5.2 The oscillating droplet

In this experiment, we study numerically the oscillation of a levitated droplet which is surrounded by a low density fluid. This is a classical problem and has been studied in detail in the literature, see [1, 39, 47, 56]. Here we consider the oscillation of a 3d

Table 2 Benchmark quantities of the rising bubble in case II.

	Stab ^h			StabV ^h		
	adapt _{5,2}	adapt _{7,3}	2adapt _{9,4}	adapt _{5,2}	adapt _{7,3}	2adapt _{9,4}
\hat{k}_{\min}	0.8117	0.7872	0.7682	0.8108	0.7873	0.7683
$t_{\hat{k}=\hat{k}_{\min}}$	1.5000	1.5000	1.5000	1.5000	1.5000	1.5000
$V_{c,\max}$	0.3621	0.3693	0.3717	0.3633	0.3693	0.3717
$t_{V_c=V_{c,\max}}$	0.6970	0.5640	0.5440	0.6180	0.5650	0.5440
$z_c(t = 1.5)$	0.9833	0.9901	0.9972	0.9831	0.9900	0.9972
$v_A(t = 1.5)$	7.94E-7	-2.68E-4	-1.17E-4	0	0	0

	Equid ^h			EquidV ^h		
	adapt _{5,2}	adapt _{7,3}	2adapt _{9,4}	adapt _{5,2}	adapt _{7,3}	2adapt _{9,4}
\hat{k}_{\min}	0.8014	0.7865	0.7682	0.8013	0.7866	0.7682
$t_{\hat{k}=\hat{k}_{\min}}$	1.5000	1.5000	1.5000	1.5000	1.5000	1.5000
$V_{c,\max}$	0.3630	0.3694	0.3717	0.3629	0.3693	0.3717
$t_{V_c=V_{c,\max}}$	0.6190	0.5640	0.5440	0.6190	0.5640	0.5440
$z_c(t = 1.5)$	0.9817	0.9901	0.9972	0.9817	0.9901	0.9972
$v_A(t = 1.5)$	1.25E-5	-1.15E-4	-9.95E-5	0	0	0

**Fig. 4** Evolution of the rising bubble in case II using the method StabV^h with 2adapt_{9,4}, where we show the generating curves of the interfaces at $t = 0, 0.3, 0.6, 1.2, 1.5$, the visualisations of the computational mesh at the final time, and the axisymmetric surface $S(t)$ at the final time $t = 1.5$ with sights in different directions.

axisymmetric droplet, with the generating curve of the initial interface of the droplet given by

$$\begin{cases} r(\theta, 0) = R_0 \left[1 + \frac{\varepsilon_0}{2} (3 \sin^2 \theta - 1) - \frac{1}{5} \varepsilon_0^2 \right] \cos(\theta), \\ z(\theta, 0) = R_0 \left[1 + \frac{\varepsilon_0}{2} (3 \sin^2 \theta - 1) - \frac{1}{5} \varepsilon_0^2 \right] \sin(\theta) + 1.0, \end{cases} \quad \theta \in \left[-\frac{\pi}{2}, \frac{\pi}{2}\right],$$

where $R_0 = 0.3$ and $\varepsilon_0 = 0.08$. For simplicity, we choose the physical parameters as

$$\rho_+ = 1, \quad \rho_- = 1000, \quad \mu_+ = 0.01, \quad \mu_- = 2, \quad \gamma = 40, \quad \vec{g} = \vec{0}.$$

The computational domain is $\mathcal{R} = [0, 0.5] \times [0, 2]$ with $\partial_1 \mathcal{R} = [0, 0.5] \times \{0, 2\}$ and $\partial_2 \mathcal{R} = \{0.5\} \times [0, 2]$. Then, on recalling [1, (15b) and (38)], we note that the dynamic

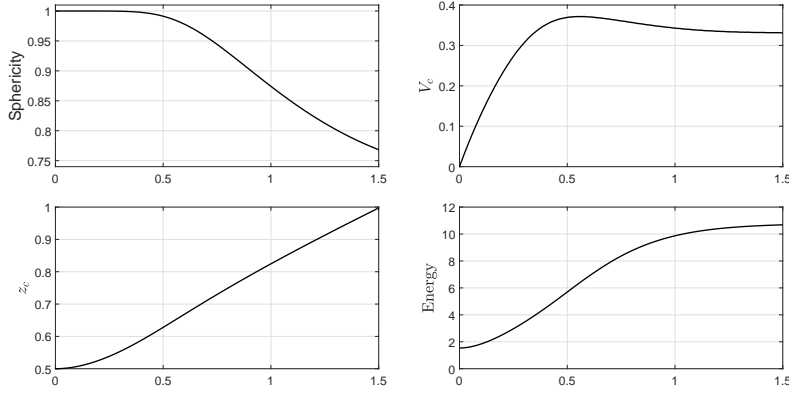


Fig. 5 The time evolution of the discrete benchmark quantities in Fig. 4.

interface of the droplet can be approximated by

$$\begin{cases} r(\theta, t) = R_0 \left[1 + \frac{\varepsilon(t)}{2} (3 \sin^2 \theta - 1) - \frac{1}{5} \varepsilon(t)^2 \right] \cos(\theta), \\ z(\theta, t) = R_0 \left[1 + \frac{\varepsilon(t)}{2} (3 \sin^2 \theta - 1) - \frac{1}{5} \varepsilon(t)^2 \right] \sin(\theta) + 1.0, \end{cases} \quad \theta \in \left[-\frac{\pi}{2}, \frac{\pi}{2}\right], \quad (5.3)$$

and $\varepsilon(t)$ is given by

$$\varepsilon(t) \approx \varepsilon_0 \exp(-\lambda_2 t) \cos(\omega_2 t) \quad \text{with} \quad \lambda_2 = \frac{5\mu_-}{\rho_- R_0^2} = \frac{1}{9}, \quad \omega_2 = \sqrt{\frac{8\gamma}{\rho_- R_0^3}} = \frac{8}{9} \sqrt{15}.$$

In Fig. 6 our obtained numerical results are compared with the approximate solution in (5.3) for the displacement of the upper endpoints of the generating curve. Here a very good agreement is observed, which demonstrates the accuracy of our introduced methods. Finally, we visualise the interface and the velocity fields in Fig. 7.

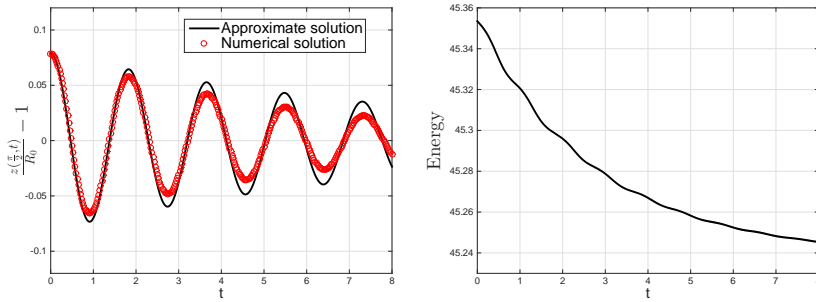


Fig. 6 The time evolution of the displacement of the upper endpoint of the generating curve on the z -axis (left panel) and the total energy (right panel), where we use `Equidh` with `2adapt9,4`.

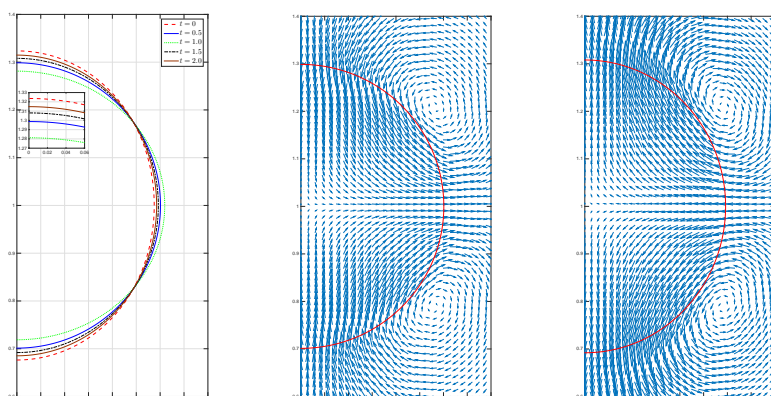


Fig. 7 Snapshots of the generating curves of the fluid interface at several times (left panel), the velocity fields at time $t = 0.5$ (middle panel) and at time $t = 1.5$ (right panel) for the experiment in Fig. 6.

6 Conclusions

We proposed four unfitted finite element methods for two-phase incompressible flow in an axisymmetric setting. The proposed methods combine an unfitted finite element method for the Navier–Stokes equation in the 2d-meridian halfplane together with a parametric finite element method in terms of the generating curve of the axisymmetric interface. We considered two different weak formulations with two possible approximations of the surface tension force. With suitable discretizations, we obtained an unconditionally stable method and a linear discretized method with the property of equidistribution. Furthermore, on utilizing suitable time-weighted discrete normals, we adapted the two introduced methods to achieve an exact volume preservation of the two phases. Numerical results were presented to show the robustness of the introduced methods and to verify these good properties.

Funding

The work of Zhao was supported by the Alexander von Humboldt Foundation.

Data availability

The datasets generated and/or analysed during the current study are available from the corresponding author on reasonable request.

Declarations

The authors certify that they have no affiliations with or involvement in any organization or entity with any financial interest or non-financial interest in the subject matter or materials discussed in this manuscript.

A Derivation of (3.11)

Let $\vec{x} = (x, y, z)$ be the Cartesian coordinates, and (r, z, φ) be the cylindrical coordinates such that

$$x = r \cos \varphi, \quad y = r \sin \varphi,$$

where $r = \sqrt{x^2 + y^2}$ is the radial distance and φ is the azimuthal angle. This gives rise to the basis vectors $\{\vec{e}_r, \vec{e}_\varphi, \vec{e}_z\}$

$$\vec{e}_r = (\cos \varphi, \sin \varphi, 0)^T, \quad \vec{e}_\varphi = (-\sin \varphi, \cos \varphi, 0)^T, \quad \vec{e}_z = (0, 0, 1)^T, \quad (\text{A.1})$$

which satisfy

$$\frac{\partial \vec{e}_r}{\partial \varphi} = \vec{e}_\varphi, \quad \frac{\partial \vec{e}_\varphi}{\partial \varphi} = -\vec{e}_r, \quad \frac{\partial \vec{e}_z}{\partial \varphi} = \vec{0}, \quad \frac{\partial \vec{e}_r}{\partial r} = \frac{\partial \vec{e}_\varphi}{\partial r} = \frac{\partial \vec{e}_z}{\partial r} = \vec{0}. \quad (\text{A.2})$$

For any scalar function $\check{b}(\vec{x})$, we write in cylindrical coordinates $b(r, \varphi, z) = \check{b}(\vec{x})$. Then we have

$$\nabla \check{b}(\vec{x}) = \frac{\partial b}{\partial r} \vec{e}_r + \frac{1}{r} \frac{\partial b}{\partial \varphi} \vec{e}_\varphi + \frac{\partial b}{\partial z} \vec{e}_z. \quad (\text{A.3})$$

For any vector-valued function $\check{\vec{b}}(\vec{x}, t)$, similarly we write $\check{\vec{b}}(\vec{x}) = \vec{b}(r, \varphi, z) = b^r \vec{e}_r + b^\varphi \vec{e}_\varphi + b^z \vec{e}_z$. Then using the relations in (A.2) gives

$$\nabla \check{\vec{b}} = [\vec{e}_r \quad \vec{e}_\varphi \quad \vec{e}_z] \begin{bmatrix} \frac{\partial b^r}{\partial r} & \frac{1}{r} \frac{\partial b^r}{\partial \varphi} - \frac{b^\varphi}{r} \frac{\partial b^r}{\partial z} \\ \frac{\partial b^\varphi}{\partial r} & \frac{b^r}{r} + \frac{1}{r} \frac{\partial b^\varphi}{\partial \varphi} & \frac{\partial b^\varphi}{\partial z} \\ \frac{\partial b^z}{\partial r} & \frac{1}{r} \frac{\partial b^z}{\partial \varphi} & \frac{\partial b^z}{\partial z} \end{bmatrix} \begin{bmatrix} (\vec{e}_r)^T \\ (\vec{e}_\varphi)^T \\ (\vec{e}_z)^T \end{bmatrix}. \quad (\text{A.4})$$

Moreover, for the divergence of $\check{\vec{b}}$ it holds that

$$\nabla \cdot \check{\vec{b}} = \frac{\partial b^r}{\partial r} \cdot \vec{e}_r + \frac{1}{r} \frac{\partial b^r}{\partial \varphi} \cdot \vec{e}_\varphi + \frac{\partial b^r}{\partial z} \cdot \vec{e}_z = \frac{\partial b^r}{\partial r} + \frac{b^r}{r} + \frac{1}{r} \frac{\partial b^\varphi}{\partial \varphi} + \frac{\partial b^z}{\partial z}. \quad (\text{A.5})$$

We now follow the axisymmetric setting in §3.1 and denote

$$\check{\vec{u}}(\vec{x}, t) = u^r(r, z, t) \vec{e}_r + u^z(r, z, t) \vec{e}_z, \quad \check{\vec{\chi}}(\vec{x}, t) = \chi^r(r, z, t) \vec{e}_r + \chi^z(r, z, t) \vec{e}_z.$$

Then it follows from (3.12a) that

$$\begin{aligned} (\rho \check{\vec{u}}, \check{\vec{\chi}})_\Omega &= 2\pi \int_{\mathcal{R}_-(t)} \rho_- (u^r \chi^r + u^z \chi^z) r \, dr dz + 2\pi \int_{\mathcal{R}_+(t)} \rho_+ (u^r \chi^r + u^z \chi^z) r \, dr dz \\ &= 2\pi \int_{\mathcal{R}} \rho_c (u^r \chi^r + u^z \chi^z) r \, dr dz = 2\pi (\rho_c \vec{u}, \vec{\chi} r), \end{aligned} \quad (\text{A.6})$$

where $\vec{u} = (u^r, u^z)^T$ and $\vec{\chi} = (\chi^r, \chi^z)^T$ are vectors in the 2d-meridian halfplane \mathcal{R} . Similarly we have

$$(\rho \partial_t \check{\vec{u}}, \check{\vec{\chi}})_\Omega = 2\pi (\rho_c \partial_t \vec{u}, \vec{\chi} r), \quad (\rho \check{\vec{u}}, \partial_t \check{\vec{\chi}})_\Omega = 2\pi (\rho_c \vec{u}, \partial_t \vec{\chi} r). \quad (\text{A.7})$$

On recalling (A.5) and (3.8), it holds that

$$(\check{q}, \nabla \cdot \check{\vec{u}}) = 2\pi \int_{\mathcal{R}} \left(\frac{\partial u^r}{\partial r} + \frac{u^r}{r} + \frac{\partial u^z}{\partial z} \right) q r \, dr dz = 2\pi (\nabla_c \cdot ([r\vec{u}], q). \quad (\text{A.8})$$

Using (A.4) for $\check{\mathbf{u}}$ and $\check{\chi}$, it is not difficult to show that

$$\int_{\Omega_{\pm}(t)} \left([\check{\mathbf{u}} \cdot \nabla] \check{\mathbf{u}} \cdot \check{\chi} - [\check{\mathbf{u}} \cdot \nabla] \check{\chi} \cdot \check{\mathbf{u}} \right) dV = 2\pi \int_{\mathcal{R}_{\pm}(t)} \left([\check{\mathbf{u}} \cdot \nabla_c] \check{\mathbf{u}} \cdot \check{\chi} - [\check{\mathbf{u}} \cdot \nabla_c] \check{\chi} \cdot \check{\mathbf{u}} \right) r \, dr dz. \quad (\text{A.9})$$

Multiplying (A.9) with ρ_{\pm} and combing these two equations gives rise to

$$\left(\rho, [\check{\mathbf{u}} \cdot \nabla] \check{\mathbf{u}} \cdot \check{\chi} - [\check{\mathbf{u}} \cdot \nabla] \check{\chi} \cdot \check{\mathbf{u}} \right)_{\Omega} = 2\pi \left(\rho_c r, [\check{\mathbf{u}} \cdot \nabla_c] \check{\mathbf{u}} \cdot \check{\chi} - [\check{\mathbf{u}} \cdot \nabla_c] \check{\chi} \cdot \check{\mathbf{u}} \right). \quad (\text{A.10})$$

Similarly we can compute

$$\underline{\mathbb{D}}(\check{\mathbf{u}}) = \frac{1}{2} \left(\nabla \check{\mathbf{u}} + (\nabla \check{\mathbf{u}})^T \right) = \begin{bmatrix} \check{e}_r & \check{e}_\varphi & \check{e}_z \end{bmatrix} \begin{bmatrix} \frac{\partial u^r}{\partial r} & 0 & \frac{1}{2} \left(\frac{\partial u^r}{\partial z} + \frac{\partial u^z}{\partial r} \right) \\ 0 & \frac{u^r}{r} & 0 \\ \frac{1}{2} \left(\frac{\partial u^r}{\partial z} + \frac{\partial u^z}{\partial r} \right) & 0 & \frac{\partial u^z}{\partial z} \end{bmatrix} \begin{bmatrix} (\check{e}_r)^T \\ (\check{e}_\varphi)^T \\ (\check{e}_z)^T \end{bmatrix}.$$

This implies that

$$\begin{aligned} & \int_{\Omega_{\pm}(t)} \underline{\mathbb{D}}(\check{\mathbf{u}}) : \underline{\mathbb{D}}(\check{\chi}) \, dV \\ &= 2\pi \int_{\mathcal{R}_{\pm}(t)} \left\{ \frac{\partial u^r}{\partial r} \frac{\partial \chi^r}{\partial r} + \frac{1}{2} \left[\frac{\partial u^r}{\partial z} + \frac{\partial u^z}{\partial r} \right] \left[\frac{\partial \chi^r}{\partial z} + \frac{\partial \chi^z}{\partial r} \right] + \frac{\partial u^z}{\partial z} \frac{\partial \chi^z}{\partial z} + \frac{u^r \chi^r}{r^2} \right\} r \, dr dz \\ &= 2\pi \int_{\mathcal{R}_{\pm}(t)} \underline{\mathbb{D}}_c(\check{\mathbf{u}}) : \underline{\mathbb{D}}_c(\check{\chi}) \, r \, dr dz + 2\pi \int_{\mathcal{R}_{\pm}(t)} (\check{\mathbf{u}} \cdot \check{\mathbf{e}}_1) (\check{\chi} \cdot \check{\mathbf{e}}_1) r^{-1} \, dr dz. \end{aligned} \quad (\text{A.11})$$

Multiplying (A.11) with μ_{\pm} and combing these two equations yields that

$$\left(\mu \underline{\mathbb{D}}(\check{\mathbf{u}}), \underline{\mathbb{D}}(\check{\chi}) \right)_{\Omega} = 2\pi \left(\mu_c r \underline{\mathbb{D}}_c(\check{\mathbf{u}}), \underline{\mathbb{D}}_c(\check{\chi}) \right) + 2\pi \left(\mu_c r^{-1} (\check{\mathbf{u}} \cdot \check{\mathbf{e}}_1), (\check{\chi} \cdot \check{\mathbf{e}}_1) \right). \quad (\text{A.12})$$

On the axisymmetric surface $S(t)$, by (3.1) we can set

$$\check{\mathbf{V}}(\check{\mathbf{x}}, t) = \check{x}_r^r \check{e}_r + \check{x}_\varphi^\varphi \check{e}_z, \quad \check{\mathbf{n}}_S(\check{\mathbf{x}}, t) = -\check{x}_s^s \check{e}_r + \check{x}_s^r \check{e}_z, \quad \check{\boldsymbol{\eta}}(\check{\mathbf{x}}) = \eta^r \check{e}_r + \eta^z \check{e}_z \quad \text{for } \check{\mathbf{x}} \in S(t). \quad (\text{A.13})$$

Denote $\zeta(\alpha, t) = \check{\zeta}(\check{\mathbf{x}}, t)$ for $\check{\mathbf{x}} \in S(t)$, $\alpha \in \mathbb{I}$. Then it is easy to get

$$\int_{S(t)} (\check{\mathbf{V}} - \check{\mathbf{u}}) \cdot \check{\mathbf{n}}_S \, \check{\zeta} \, dS = 2\pi \int_{\Gamma(t)} (\check{\mathbf{x}}_t - \check{\mathbf{u}}) \cdot \check{\mathbf{v}} \, \zeta(\check{\mathbf{x}} \cdot \check{\mathbf{e}}_1) \, ds = 2\pi \left\langle (\check{\mathbf{x}} \cdot \check{\mathbf{e}}_1) (\check{\mathbf{x}}_t - \check{\mathbf{u}}) \cdot \check{\mathbf{v}}, \zeta | \check{\mathbf{x}}_\alpha \right\rangle. \quad (\text{A.14})$$

Similarly, it is straightforward to obtain

$$\int_{S(t)} \mathcal{H} \check{\mathbf{n}}_S \cdot \check{\boldsymbol{\eta}} \, dS = 2\pi \int_{\Gamma(t)} \kappa \check{\mathbf{v}} \cdot \check{\boldsymbol{\eta}} (\check{\mathbf{x}} \cdot \check{\mathbf{e}}_1) \, ds = 2\pi \left\langle (\check{\mathbf{x}} \cdot \check{\mathbf{e}}_1) \kappa \check{\mathbf{v}}, \check{\boldsymbol{\eta}} | \check{\mathbf{x}}_\alpha \right\rangle, \quad (\text{A.15})$$

where $\check{\boldsymbol{\eta}} = (\eta^r, \eta^z)^T$ is the vector in the 2d-meridian plane. Finally, we have

$$\begin{aligned} \int_{S(t)} \nabla_s \check{\mathbf{u}} : \nabla_s \check{\boldsymbol{\eta}} \, dS &= \int_{S(t)} \nabla_s \cdot \check{\boldsymbol{\eta}} \, dS = 2\pi \int_{\Gamma(t)} (\check{\mathbf{x}} \cdot \check{\mathbf{e}}_1) \left(\check{\mathbf{x}}_s \cdot \check{\boldsymbol{\eta}}_s + \frac{\check{\boldsymbol{\eta}} \cdot \check{\mathbf{e}}_1}{\check{\mathbf{x}} \cdot \check{\mathbf{e}}_1} \right) ds \\ &= 2\pi \int_{\mathbb{I}} (\check{\mathbf{x}} \cdot \check{\mathbf{e}}_1) \check{\mathbf{x}}_s \cdot \check{\boldsymbol{\eta}}_s | \check{\mathbf{x}}_\alpha | + (\check{\boldsymbol{\eta}} \cdot \check{\mathbf{e}}_1) | \check{\mathbf{x}}_\alpha | \, d\alpha, \end{aligned} \quad (\text{A.16})$$

where we used the fact

$$\nabla_s \cdot \check{\boldsymbol{\eta}} = \check{x}_s^r \eta_s^r + \check{x}_s^z \eta_s^z + \frac{\eta^r}{\check{\mathbf{x}} \cdot \check{\mathbf{e}}_1}. \quad (\text{A.17})$$

Collecting the above results, we obtain (3.11) from (2.6).

References

1. A. Aalilija, C.A. Gandin, E. Hachem, On the analytical and numerical simulation of an oscillating drop in zero-gravity, *Comput. Fluids* 197 (2020) 104362.
2. M. Agnese, R. Nürnberg, Fitted front tracking methods for two-phase incompressible Navier–Stokes flow: Eulerian and ALE finite element discretizations, *Int. J. Numer. Anal. Mod.* 17 (2020) 613–642.
3. D.M. Anderson, G.B. McFadden, A.A. Wheeler, Diffuse-interface methods in fluid mechanics, *Annu. Rev. Fluid Mech.* 30 (1998) 139–165.
4. G. Anjos, N. Mangiavacchi, N. Borhani, J.R. Thome, 3D ALE finite-element method for two-phase flows with phase change, *Heat Transf. Engrg.* 35 (2014) 537–547.
5. E. Bänsch, Finite element discretization of the Navier–Stokes equations with a free capillary surface, *Numer. Math.* 88 (2001) 203–235.
6. W. Bao, H. Garcke, R. Nürnberg, Q. Zhao, Volume-preserving parametric finite element methods for axisymmetric geometric evolution equations, *J. Comput. Phys.* 460 (2022) 111180.
7. W. Bao, Q. Zhao, A structure-preserving parametric finite element method for surface diffusion, *SIAM J. Numer. Anal.* 59 (2021) 2775–2799.
8. J.W. Barrett, H. Garcke, R. Nürnberg, A parametric finite element method for fourth order geometric evolution equations, *J. Comput. Phys.* 222 (2007) 441–467.
9. J.W. Barrett, H. Garcke, R. Nürnberg, On stable parametric finite element methods for the Stefan problem and the Mullins–Sekerka problem with applications to dendritic growth, *J. Comput. Phys.* 229 (2010) 6270–6299.
10. J.W. Barrett, H. Garcke, R. Nürnberg, Eliminating spurious velocities with a stable approximation of viscous incompressible two-phase Stokes flow, *Comput. Methods Appl. Mech. Engrg.* 267 (2013) 511–530.
11. J.W. Barrett, H. Garcke, R. Nürnberg, A stable parametric finite element discretization of two-phase Navier–Stokes flow, *J. Sci. Comput.* 63 (2015) 78–117.
12. J.W. Barrett, H. Garcke, R. Nürnberg, Finite element methods for fourth order axisymmetric geometric evolution equations, *J. Comput. Phys.* 376 (2019) 733–766.
13. J.W. Barrett, H. Garcke, R. Nürnberg, Variational discretization of axisymmetric curvature flows, *Numer. Math.* 141 (2019) 791–837.
14. J.W. Barrett, H. Garcke, R. Nürnberg, Parametric finite element approximations of curvature driven interface evolutions, *Handb. Numer. Anal.* (Andrea Bonito and Ricardo H. Nochetto, eds.) 21 (2020) 275–423.
15. Z. Belhachmi, C. Bernardi, S. Deparis, Weighted Clément operator and application to the finite element discretization of the axisymmetric Stokes problem, *Numer. Math.* 105 (2006) 217–247.
16. C. Bernardi, M. Dauge, Y. Maday, *Spectral Methods for Axisymmetric Domains*, volume 3, Gauthier-Villars, Éditions Scientifiques et Médicales Elsevier, Paris, 1999.
17. J. Chessa, T. Belytschko, An enriched finite element method and level sets for axisymmetric two-phase flow with surface tension, *Int. J. Numer. Methods Engrg.* 58 (2003) 2041–2064.
18. S.W. Cheung, E. Chung, H.H. Kim, A mass conservative scheme for fluid–structure interaction problems by the staggered discontinuous Galerkin method, *J. Sci. Comput.* 74 (2018) 1423–1456.
19. B. Duan, B. Li, Z. Yang, An energy diminishing arbitrary Lagrangian–Eulerian finite element method for two-phase Navier–Stokes flow, *J. Comput. Phys.* 461 (2022) 111215.
20. G. Dziuk, An algorithm for evolutionary surfaces, *Numer. Math.* 58 (1990) 603–611.
21. X. Feng, Fully discrete finite element approximations of the Navier–Stokes–Cahn–Hilliard diffuse interface model for two-phase fluid flows, *SIAM J. Numer. Anal.* 44 (2006) 1049–1072.
22. T. Frachon, S. Zahedi, A cut finite element method for incompressible two-phase Navier–Stokes flows, *J. Comput. Phys.* 384 (2019) 77–98.
23. S. Ganesan, *Finite element methods on moving meshes for free surface and interface flows*, Ph.D. thesis, University Magdeburg, Magdeburg, Germany, 2006.
24. S. Ganesan, L. Tobiska, An accurate finite element scheme with moving meshes for computing 3D-axisymmetric interface flows, *Int. J. Numer. Methods Fluids* 57 (2008) 119–138.
25. H. Garcke, M. Hinze, C. Kahle, A stable and linear time discretization for a thermodynamically consistent model for two-phase incompressible flow, *Appl. Numer. Math.* 99 (2016) 151–171.
26. H. Garcke, R. Nürnberg, Q. Zhao, Structure-preserving discretizations of two-phase Navier–Stokes flow using fitted and unfitted approaches, *J. Comput. Phys.* 489 (2023) 112276.

27. F. Gibou, R. Fedkiw, S. Osher, A review of level-set methods and some recent applications, *J. Comput. Phys.* 353 (2018) 82–109.
28. E. Gros, G.R. Anjos, J.R. Thome, Interface-fitted moving mesh method for axisymmetric two-phase flow in microchannels, *Int. J. Numer. Methods Fluids* 86 (2018) 201–217.
29. S. Groß, A. Reusken, An extended pressure finite element space for two-phase incompressible flows with surface tension, *J. Comput. Phys.* 224 (2007) 40–58.
30. S. Groß, A. Reusken, Numerical methods for two-phase incompressible flows, volume 40 of *Springer Series in Computational Mathematics*, Springer-Verlag, Berlin, 2011.
31. G. Grün, F. Klingbeil, Two-phase flow with mass density contrast: stable schemes for a thermodynamic consistent and frame-indifferent diffuse-interface model, *J. Comput. Phys.* 257 (2014) 708–725.
32. C.W. Hirt, B.D. Nichols, Volume of fluid (VOF) method for the dynamics of free boundaries, *J. Comput. Phys.* 39 (1981) 201–225.
33. J. Hu, B. Li, Evolving finite element methods with an artificial tangential velocity for mean curvature flow and Willmore flow, *Numer. Math.* 152 (2022) 127–181.
34. F. Huang, W. Bao, T. Qian, Diffuse-interface approach to competition between viscous flow and diffusion in pinch-off dynamics, *Phys. Rev. Fluids* 7 (2022) 094004.
35. T.J. Hughes, W.K. Liu, T.K. Zimmermann, Lagrangian-Eulerian finite element formulation for incompressible viscous flows, *Comput. Methods Appl. Mech. Engrg.* 29 (1981) 329–349.
36. S.R. Hysing, S. Turek, D. Kuzmin, N. Parolini, E. Burman, S. Ganesan, L. Tobiska, Quantitative benchmark computations of two-dimensional bubble dynamics, *Int. J. Numer. Methods Fluids* 60 (2009) 1259–1288.
37. W. Jiang, B. Li, A perimeter-decreasing and area-conserving algorithm for surface diffusion flow of curves, *J. Comput. Phys.* 443 (2021) 110531.
38. J. Kim, A diffuse-interface model for axisymmetric immiscible two-phase flow, *Appl. Math. Comput.* 160 (2005) 589–606.
39. H. Lamb, On the oscillations of a viscous spheroid, *Proceedings of the London Mathematical Society* 1 (1881) 51–70.
40. C. M. Elliott, H. Fritz, On approximations of the curve shortening flow and of the mean curvature flow based on the DeTurck trick, *IMA J. Numer. Anal.* 37 (2017) 543–603.
41. S. Mirjalili, S.S. Jain, M. Dodd, Interface-capturing methods for two-phase flows: An overview and recent developments, *CTR Ann. Res. Briefs* 2017 (2017) 13.
42. E. Olsson, G. Kreiss, S. Zahedi, A conservative level set method for two phase flow II, *J. Comput. Phys.* 225 (2007) 785–807.
43. S. Osher, R. Fedkiw, *Level Set Methods and Dynamic Implicit Surfaces*, volume 153, Springer Science & Business Media, 2002.
44. B. Perot, R. Nallapati, A moving unstructured staggered mesh method for the simulation of incompressible free-surface flows, *J. Comput. Phys.* 184 (2003) 192–214.
45. S. Popinet, An accurate adaptive solver for surface-tension-driven interfacial flows, *J. Comput. Phys.* 228 (2009) 5838–5866.
46. S. Quan, D.P. Schmidt, A moving mesh interface tracking method for 3D incompressible two-phase flows, *J. Comput. Phys.* 221 (2007) 761–780.
47. L. Rayleigh, et al., On the capillary phenomena of jets, *Proc. R. Soc. London* 29 (1879) 71–97.
48. Y. Renardy, M. Renardy, PROST: a parabolic reconstruction of surface tension for the volume-of-fluid method, *J. Comput. Phys.* 183 (2002) 400–421.
49. A. Schmidt, K.G. Siebert, Design of Adaptive Finite Element Software: The Finite Element Toolbox ALBERTA, volume 42 of *Lecture Notes in Computational Science and Engineering*, Springer-Verlag, Berlin, 2005.
50. J.A. Sethian, *Level set methods and fast marching methods: evolving interfaces in computational geometry, fluid mechanics, computer vision, and materials science*, volume 3, Cambridge university press, 1999.
51. V. Styles, D. Kay, R. Welford, Finite element approximation of a Cahn–Hilliard–Navier–Stokes system, *Interfaces Free Bound.* 10 (2008) 15–43.
52. M. Sussman, E.G. Puckett, A coupled level set and volume-of-fluid method for computing 3D and axisymmetric incompressible two-phase flows, *J. Comput. Phys.* 162 (2000) 301–337.
53. M. Sussman, P. Smereka, S. Osher, A level set approach for computing solutions to incompressible two-phase flow, *J. Comput. Phys.* 114 (1994) 146–159.

-
54. G. Tryggvason, B. Bunner, A. Esmaeeli, D. Juric, N. Al-Rawahi, W. Tauber, J. Han, S. Nas, Y.J. Jan, A front-tracking method for the computations of multiphase flow, *J. Comput. Phys.* 169 (2001) 708–759.
 55. S.O. Unverdi, G. Tryggvason, A front-tracking method for viscous, incompressible multi-fluid flows, *J. Comput. Phys.* 100 (1992) 25–37.
 56. R. Velentine, N. Sather, W. Heideger, The motion of drops in viscous media, *Chem. Engrg. Sci.* 20 (1965) 719–728.
 57. Q. Zhao, W. Ren, An energy-stable finite element method for the simulation of moving contact lines in two-phase flows, *J. Comput. Phys.* 417 (2020) 109582.